Supplemental Information

Mechanisms of Allosteric Gene Regulation by NMR Quantification of μs-ms Protein Dynamics

Ian R Kleckner[a], Paul Gollnick[b], Mark P Foster[c‡]

[a]Biophysics Program, Ohio State University, 484 West 12th Ave, Columbus, OH 43210; ian.kleckner@gmail.com

[b]Department of Biological Sciences, University at Buffalo, the State University of New York, Buffalo, NY 14260; gollnick@buffalo.edu

[c]Biochemistry Department, Ohio State University, 484 West 12th Ave , Columbus, OH 43210

[‡]Corresponding author: 484 West 12th Ave , Columbus, OH, 43210, USA. Phone: (614) 292-1377; Fax: (614) 292-6773; Foster.281@osu.edu

Supplemental materials and methods

Sample preparation. *B. stearothermophilus* TRAP mutagenesis, expression, and purification protocols were described previously [1]. Residue numbers used correspond to those of *B. subtilis* TRAP, matching the scheme used in the crystal structure of *B. stearothermophilus* TRAP (1C9S and 3AQD); they therefore differ by +2 from to the native *B. stearothermophilus* sequence. Mutagenesis was performed using the Stratagene QuikChange method using a plasmid clone [1] with the WT *B. stearothermophilus* gene and oligonucleotide primers designed to change Ala 28 to Ile. Candidate clones were sequenced by the Roswell Park Biopolymers sequencing facility and a clone with the desired substitutions was transformed into *E. coli* BL21(DE3). NMR spectra indicate this mutation does not significantly alter the structure of WT TRAP (Fig. S1), additional studies report no significant change in μs-ms dynamics (Fig. S3), and the mutation does not significantly affect Trp binding (data not shown). In this work, "TRAP" refers to *B. stearothermophilus* A28I TRAP, unless specified.

To ensure homogeneous apo protein, solid guanidinium hydrochloride (GdnHCl) was added up to 6M concentration to a 1-2 mg/mL TRAP sample in NMR buffer, 100 mM NaCl, 50 mM $NaPO_4$, pH 8.0 at 25°C, 0.02% NaN_3. This solution was filtered using a 0.45 μm syringe filter. Several 5-15 mg aliquots of TRAP were purified via reversed-phase HPLC (Vydac protein C4 column model 214TP1010 at 5.0 mL/min, using a linear gradient from 20-80% acetonitrile (AcN) in H_2O / 0.1% trifluoroacetic acid over 40 min). Free Trp elutes at < 10% AcN, and apo TRAP elutes in multiple overlapping peaks at 30-40% AcN, the purity of which were verified by matrix-assisted laser desorption/ionization mass spectrometry. Purified apo TRAP

samples were frozen, lyophilized, and resuspended in NMR buffer with 6M GdnHCl at a concentration of 1-2 mg/mL in 5-10 mL in a 3 kDa- or 8 kDa-cutoff dialysis membrane or cassette (Thermo Scientific model 66333 Slide-A-Lyzer). The donut was re-assembled by step-wise dilution of GdnHCl via dialysis for 4-12 hrs per step: (1) 0.5 L of 3M GdnHCl in NMR buffer at 55°C, (2) 1 L of 1.5M GdnHCl in NMR buffer at 55°C, (3) 1 L of NMR buffer at 55°C (4) 1 L of NMR buffer at 25°C (5) 1 L of NMR buffer at 25°C. This sample was concentrated using either 3 kDa- or 8 kDa-cutoff centrifugal filter unit (Amicon Ultra-4) at 5,000 RPM. Any precipitation was isolated and discarded via centrifugation. The TRAP concentration was quantified using UV absorbance at 280 nm with ε = 2,980 /M/cm, calculated using ProtParam [2]. Trp solutions were prepared by adding solid Trp to NMR buffer, and concentration was quantified by absorbance at 278 nm with extinction coefficient ε = 5,579 /M/cm [3]. To prepare D_2O-based samples for NMR relaxation experiments, H_2O samples were weighed using an analytical balance to estimate water volume, lyophilized, and resuspended with an equivalent volume of 99.99% D_2O (Cambridge Isotope Labs).

Protein samples with three distinct isotope labeling schemes were used for this study: (1) Total Correlation SpectroscopY (TOCSY) and out-and-back spectra utilized a sample with labeling scheme U-[^{2}H, ^{13}C, ^{15}N], ILV-[$^{13}CH_3$] to permit magnetization transfer from side chain to backbone [4], (2) stereo-assignments required the labeling scheme 10%-[^{13}C] to enable stereo-specific carbon-carbon coupling [5], and (3) MRD spectra utilized labeling scheme U-[^{2}H, ^{15}N], ILV-[$^{13}CH_3$] to prevent spurious dispersions from carbon-carbon coupling [6]. All assignment spectra used 600-900 μM WT TRAP 11-mer in H_2O NMR buffer to observe $^{1}H^{N}$

signals. MRD spectra used 130-145 μM A28I TRAP 11-mer in D_2O NMR buffer to minimize both ^1H_2O signal and unwanted ^1H-based relaxation enhancement. Trp-saturated (holo) TRAP samples were confirmed by observation of free Trp signals in the 1D ^1H- NMR spectrum achieved at ~2:1 Trp:TRAP monomer (n.b., TRAP-Trp K_d ~ 10 μM [7]).

Molecular visualization. Pymol (http://pymol.sourceforge.net) was used to generate figures and apply A26I in silico mutation to 1C9S [8]. Qutemol (http://qutemol.sourceforge.net; [9]) was used to generate fig. S1. Structural groupings listed in fig. S6 and table S1 were assigned using GETAREA [10].

NMR spectroscopy. Apo and holo WT TRAP methyl signals were assigned using several experiments, two NMR samples, and backbone $^1H^N$ and ^{15}N assignments [1], all at 50-55°C. Assignments were transferred from WT to A28I TRAP by spectral comparison (Fig. S2). Assignments of apo TRAP were obtained from six NMR spectra, all acquired using a Bruker DRX-600 equipped with a cryoprobe: (1) 3D C(CO)NH-TOCSY using 14.7 ms DIPSI mixing time at B_1 = 9.6 kHz with (32, 8, 512) complex points over (3018, 1703, 7183) Hz SW using 192 scans, (2) 3D H(CCO)NH-TOCSY using 14.7 ms DIPSI mixing time at B_1 = 9.6 kHz with (32, 8, 512) complex points over (1801, 1703, 7183) Hz SW using 192 scans, (3, 4, 5) 2D methyl “out and back” [4] correlating (C^{m-x}, H^m) where x = {0, 1, 2} is the number of C-C magnetization-transfers from methyl carbon towards backbone with (128, 1024) complex points over (10565, 2404) Hz SW using 16 scans, (6) 2D ^{13}C-edited ^1H-^1H NOESY using 300 ms mixing time with (128, 1024) complex points over (3018,

8993) Hz SW using 64 scans.

Holo TRAP methyls were assigned from five NMR spectra, recorded at University of Toronto using a Varian Inova 500 MHz spectrometer equipped with room temperature probe: (1) 3D C(CO)NH-TOCSY using 23.7 ms DIPSI mixing time at B_1 = 7.0 kHz with (18, 52, 511) complex points over (1800, 1450, 8000) Hz SW using 32 scans, (2) 3D H(CCO)NH-TOCSY using 23.7 ms DIPSI mixing time at B_1 = 7.0 kHz with (16, 52, 511) complex points over (1000, 1450, 8000) Hz SW using 32 scans, (3, 4, 5) 3D methyl "out and back" [4] correlating (C^{m-x}, H^m) where x = {0, 1, 2} with (24, 50, 400) complex points over (1800, 5000, 8000) Hz SW using 4 scans.

Stereo-specific assignments for apo and holo TRAP were obtained from a non-decoupled ^{1}H-^{13}C HSQC spectrum recorded on a Bruker DRX-800 equipped with a cryoprobe with (256, 1024) complex points over (4024, 10417) Hz SW using 32 scans. Doublet signals split via J-coupling were assigned as Pro-(R), methyl group number 1, and singlet signals were assigned as Pro-(S), methyl group number 2 [5].

Dispersions for each of 4 MRD conditions consisted of 12 2D spectra: one reference with $T = \nu_{CPMG} = 0$, and 11 CPMG with T = 20 ms acquired in random order using ν_{CPMG} = 100, 200, 300, 400, 500, 600, 700, 800, 900, 1000, 1000 Hz. The 4 MRD conditions utilized ^{1}H,^{13}C-MQ [11] with two ^{13}C carriers [11], or ^{13}C-SQ [12]: (1) 25°C, 800 MHz, MQ, (2) 25°C, 800 MHz, SQ (apo and holo), (3) 25°C, 600 MHz, MQ, and (4) 25°C, 600 MHz, SQ. MRD spectra utilized (96, 512) complex points over (16, 3) ppm SW with the ^{1}H carrier at 1 ppm, and ^{13}C carrier at either 19 ppm (SQ), 14 ppm (MQ, Ile region), or 22 ppm (MQ, Leu and Val region), where distinct ^{13}C carriers are selected to minimize off-resonance effects [11]. SQ spectra used 16

scans and required 103 min/spectrum, and MQ data utilized 8 scans and required 53 min/spectrum. Data processing, assignment, and display were performed using NMRPipe [13] and NMRViewJ [14]. Temperatures were calibrated with ethylene glycol, and chemical shifts referenced with 4,4-dimethyl-4-silapentane-1-sulfonic acid (DSS) in matched buffer (n.b., DSS binds to TRAP; Ian Kleckner and Philipp Neudecker (Univ. Toronto), unpublished results).

MRD analysis. MRD curves quantify the relationship between applied refocusing frequency ν_{CPMG} and effective transverse relaxation rate $R_2^{Eff} = -\ln\left(I(\nu_{CPMG}) / I_0 \right) / T_{CPMG}$, where $I(\nu_{CPMG})$ is the signal intensity in the 2D spectrum acquired with refocusing frequency ν_{CPMG}, I_0 is the reference signal intensity obtained in the spectrum with no refocusing block, and T_{CPMG} is the duration of the refocusing block. Intensities of NMR crosspeaks were extracted from simulated peak shapes using the autoFit.tcl package from nmrPipe [13] and errors in intensities $\sigma(R_2^{Eff})$ were estimated via standard deviation from repeat measures of $I(\nu_{CPMG})$.

The following procedure for analysis of the MRD was implemented using the software GUARDD (Kleckner, et al., in preparation; http://code.google.com/p/guardd/), written in-house using MATLAB (The Mathworks, Inc.). Dispersion curves were fit to Carver-Richards-style formulae that describe two-site exchange A↔B for MQ or SQ dispersions. The fitting equations for multiple quantum (MQ) dispersions, which simplify to single quantum (SQ) dispersions provided $\Delta\omega_H = 0$, are as follows using $\delta = 1 / (4\nu_{CPMG})$ and $n = T_{CPMG}\nu_{CPMG}$ [11, 15]:

$$R_2^{Eff}\left(\frac{1}{2\delta}\right) = \Re(\lambda_1) - \frac{\ln(Q)}{4n\delta} \quad (1a)$$

$$\lambda_1 = R_2^0 + \frac{1}{2}\left(k_{ex} - \left(\frac{1}{2\delta}\right)\cosh^{-1}\left(D_+\cosh(\eta_+) - D_-\cos(\eta_-)\right)\right) \quad (1b)$$

$$D_\pm = \frac{1}{2}\left(\frac{\Psi + 2\Delta\omega_X^2}{(\Psi^2+\varsigma^2)^{1/2}} \pm 1\right) \quad (1c)$$

$$\eta_\pm = \sqrt{2}\,\delta\left((\Psi^2+\varsigma^2)^{1/2} \pm \Psi\right)^{1/2} \quad (1d)$$

$$\Psi = \left(i\Delta\omega_H + (P_A - P_B)k_{ex}\right)^2 - \Delta\omega_C^2 + 4P_AP_Bk_{ex}^2 \quad (1e)$$

$$\varsigma = -2\Delta\omega_C\left(i\Delta\omega_H + (P_A - P_B)k_{ex}\right) \quad (1f)$$

$$Q = \Re\left(1 - m_D^2 + m_Dm_Z - m_Z^2 + \left(\frac{m_D+m_Z}{2}\right)\left(\frac{P_B}{P_A}\right)^{1/2}\right) \quad (1g)$$

$$m_D = \frac{ik_{ex}(P_AP_B)^{1/2}}{d_+z_-}\left(z_+ + 2\Delta\omega_C\left(\frac{\sin(z_+\delta)}{\sin((d_+ + z_+)\delta)}\right)\right) \quad (1h)$$

$$m_Z = \frac{ik_{ex}(P_AP_B)^{1/2}}{d_-z_-}\left(d_- - 2\Delta\omega_C\left(\frac{\sin(d_-\delta)}{\sin((d_- + z_-)\delta)}\right)\right) \quad (1i)$$

$$d_\pm = (\Delta\omega_H + \Delta\omega_C) \pm ik_{ex} \quad (1j)$$

$$z_\pm = (\Delta\omega_H - \Delta\omega_C) \pm ik_{ex} \quad (1k)$$

Each curve requires specification of 5 types of parameters: (1, 2) $|\Delta\omega_H|$ and $|\Delta\omega_C|$, the ppm magnitude of ^{1}H and ^{13}C chemical shift differences between states A and B (note: $|\Delta\omega_H|$ is fixed to zero only for ^{13}C-SQ curves), which are converted from ppm to rad/s for each curve via $\Delta\omega_X^{(rad/sec)} = 2\pi\gamma_X B_0 \Delta\omega_X^{(ppm)}$, where γ_X is the gyromagnetic ratio for nucleus X (e.g., ^{1}H, ^{13}C), (3) P_A, the equilibrium population fraction of state A, (4) $k_{ex} = k_A + k_B$, the rate of exchange between states A and B. k_A

and k_B are the rates of exchange from A→B and B→A, respectively, with k_A = (1-P_A)k_{ex} and $k_B = P_A k_{ex}$. (5) R_2^0 , the transverse relaxation rate in the absence of exchange assuming $R_2^0 = R_{2A}^0 \approx R_{2B}^0$ [15, 16].

When fitting multiple dispersion curves, these 5 parameters were shared by way of three different models. (A) The site-specific model aggregates up to all four curves from a single NMR probe into a group (e.g., Ile 28δ_1), and optimizes shared values of $|\Delta\omega_H|$, $|\Delta\omega_C|$, P_A, and k_{ex} for all curves, as well as one R_2^0 for each curve. (B) The group-optimized model aggregates curves from multiple NMR probes into a group (e.g., Ile 28δ_1 + Leu 24δ_1), with variable P_A and k_{ex} used for all curves in the group, and variable $|\Delta\omega_H|$ and $|\Delta\omega_C|$ for each set of curves from the same NMR probe, and one variable R_2^0 for each curve. (C) The group-fixed model is the same as (B) except that P_A and k_{ex} are fixed for all curves in the group, instead of being variable fitted parameters (because, for large groups, varying P_A and k_{ex} in addition to site-specific $|\Delta\omega|$ makes it difficult to find the global minimum of χ^2).

RD data can be challenging to interpret because of their multivariate nature [17, 18], and because P_A and $\Delta\omega$ are unknown if the NMR probe is in the fast-exchange regime ($k_{ex} >> \Delta\omega$, or $\alpha \rightarrow 2.0$, where α = d(ln(R_{ex})) / d(ln($\Delta\omega$)) [19]). Hence, to assess the sensitivity of the final fit to initial conditions, the data in each group for models (A) and (B) were fit multiple times using a grid search over 4D parameter space which varies $|\Delta\omega_H|$ from [0.01, 0.1] ppm in 2 steps, $|\Delta\omega_C|$ from [0.1, 2.0] ppm in 3 steps, P_A from [0.8, 0.999] in 4 steps and k_{ex} from [500, 3,500] /s in 4 steps. Each grid point specified starting conditions for the fit optimization, which used the *fmincon* function from MATLAB to minimize the target function

$\chi^2 = \sum_{\text{All obs}} \left(\frac{R_{2,Eff}^{\text{Obs}}(\vec{\text{Obs}}) - R_{2,Eff}^{\text{Calc}}(\vec{\text{Obs}}, \vec{p})}{\sigma(R_{2,Eff}^{\text{Obs}}(\vec{\text{Obs}}))} \right)^2$ where $\vec{\text{Obs}}$ designates the set of experimental conditions ν_{CPMG} and B_0, and $\vec{p}$ designates the independent fitting parameters for the group: {$|\Delta\omega_H|$(Probe), $|\Delta\omega_C|$(Probe)}, P_A, k_{ex}, and $\{R_2^0(\text{Curve})\}$. For each group, goodness of fit is assessed by visual inspection of the χ^2 map resulting from the grid search. Fits were deemed reasonable if the same fitting solution (same χ^2 and parameter values, within 5%) was achieved in at least 30% of the initial conditions sampled from the grid search, or if the other candidate solutions appeared unreasonable from visually inspecting the curve fit. For many probes, fast-exchange precluded knowledge of P_A, $|\Delta\omega_H|$, and $|\Delta\omega_C|$, as evidenced by a wide range in parameter values that yield equivalent quality of fit, assessed via χ^2, as well as the calculated value of α approaching 2.0. Despite ill-defined parameters, R_{ex} can often be reliably estimated for each curve as $R_{\text{ex}} \approx R_{2,Eff}^{Fit}(\nu_{CPMG} \approx 0\,\text{Hz}) - R_{2,Eff}^{Fit}(\nu_{CPMG} \approx 10^4\,\text{Hz})$. However, some fits over-estimated R_{ex} (e.g., Val 21γ_2; Fig S4), and therefore were manually reduced based on the $R_{2,Eff}$ values observed at 100 Hz and 1000 Hz.

Errors in fitted parameters are estimated by Monte Carlo "bootstrapping" from fit residuals [20]. Residuals are calculated for each observed ν_{CPMG} value in a given dispersion curve as $\epsilon(\nu_{CPMG}) = R_{2,Eff}^{\text{Obs}}(\nu_{CPMG}) - R_{2,Eff}^{\text{Calc}}(\nu_{CPMG})$. The set of residuals is used to create a normal distribution $\boldsymbol{N}(mean(\vec{\epsilon}), var(\vec{\epsilon}))$ for the dispersion curve. A synthetic dispersion *curve* is then created using the best fit values at each observed ν_{CPMG} and a random sample from this normal distribution: $R_{2,Eff}^{\text{Synth}}(\nu_{CPMG}) = R_{2,Eff}^{\text{Calc}}(\nu_{CPMG}) + Sample[\,\boldsymbol{N}(mean(\vec{\epsilon}), var(\vec{\epsilon}))\,]$. This is repeated for

each curve in the group such that a synthetic dataset is produced. The synthetic group is fit using initial conditions set to the best fit of the actual data. This process is repeated 100 times to create 100 synthetic datasets and 100 sets of optimized fit parameters. The error in a given parameter is estimated as the standard deviation of the optimized fit parameter from its 100 element distribution. For the current dataset, this entire procedure required 30-300 min for each group on a desktop PC with a 2.6 GHz CPU and 3 Gb of RAM running MATLAB R2011a.

Table legends

Table S1. List of 29 probed sidechain atoms, interactions in holo TRAP, and hypothesized site-specific models for apo TRAP structure and dynamics.

(a) Reside numbering in crystal structure 1C9S uses *B. subtilis* sequence (i.e., add 2 to the native *B. stearothermophilus* residue number).

(b) Distances are closest carbon-to-carbon measured using Pymol [21].

(c) C(Me) SAS designates surface probe accessibility for the methyl carbon, calculated using GETAREA on the modified A28I/1C9S coordinate set, without hydrogens [10].

(d) “Nbr” designates the residue is on the protomer neighboring the probe.

(e) “Self “ designates the residue is on the same protomer as the probe.

(f) ^{1}H shift differences $\Delta\delta_H$ and $\Delta\omega_H$ are influenced by local magnetic shielding by electron density on nearby charged and aromatic moieties.

(g) ^{13}C chemical shift differences $\Delta\delta_C$ and $\Delta\omega_C$ report the magnitude of structural change, and can reflect alterations to sidechain rotameric state (e.g., packing).

(h) Exchange rate constant $k_{ex} = k_A + k_B$.

(i) Quantities listed are as percent of the observed maximum. Descriptors "small," "modest," and "large" refer to ranges 0-20%, 20-60%, and 60-100%, respectively.

Table S2. Parameter values from MRD analysis, both site-specific fits and group-wise fits are shown.

(a) "Best Fit OK?" indicates whether the χ^2 map is reasonable based on visual inspection, to assess the sensitivity of the final fit to the initial conditions.

(b) "DoF" designates the degrees of freedom, the number of observations minus number of model parameters.

(c) "NoEx" designates the no exchange model (i.e., $R_{ex} = 0$).

(d) "Ex" designates the two-state exchange model described in the text.

(e) "χ^2Red" designates the reduced chi squared value, equal to χ^2 / *DoF.*

(f) "F(Ex)" designates the statistical F-value, equal to χ^2*Red*(NoEx) / χ^2*Red*(Ex).

(g) "P(Ex)" designates the P-value which corresponds to probability of obtaining the F(Ex) value from the F-distribution (smaller value more strongly favors "Ex" model).

Figure legends

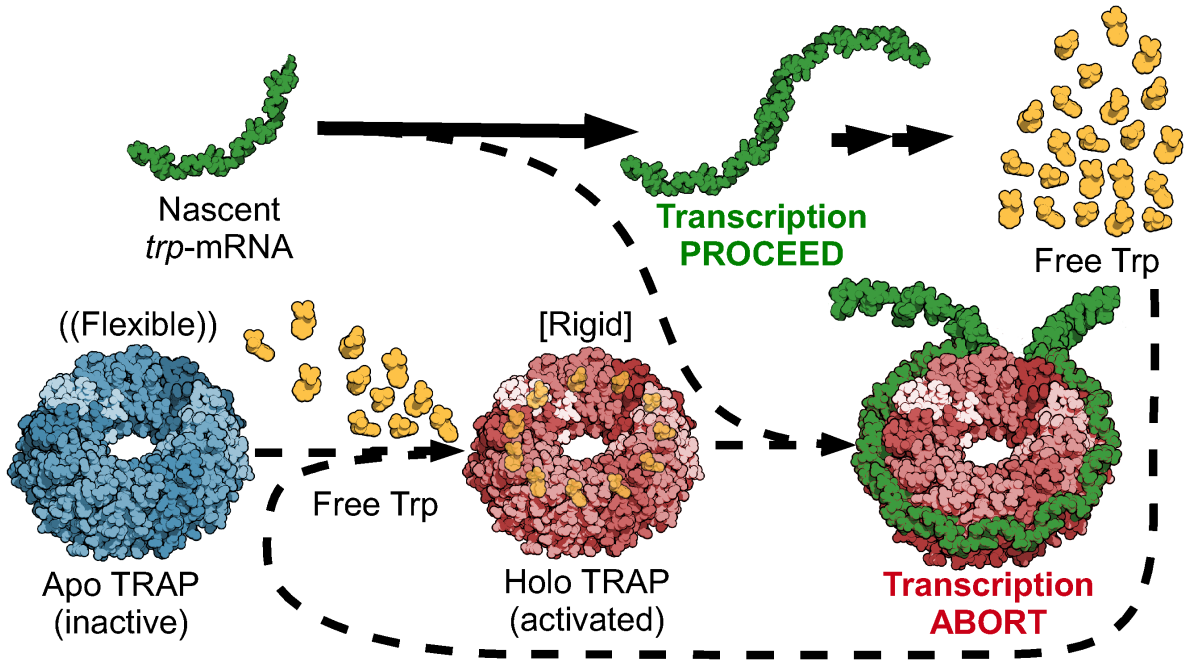

Fig. S1. The *trp* RNA-binding attenuation protein (TRAP) is a paradigmatic switch-like protein utilized by certain bacilli for regulation of the tryptophan (Trp) biosynthetic genes associated with the *trp* operon. (a) When free Trp concentration is low, TRAP is free and inactive (apo) and transcription of the *trp*-mRNA proceeds unattenuated, the encoded proteins are translated (not shown), and free Trp is synthesized. When free Trp concentration is high, apo TRAP binds up to 11 Trp molecules (now designated “holo”), and is subsequently activated for binding the *trp*-mRNA target via changes in structure and reduction in μs-ms flexibility. The nascent *trp*-mRNA wraps around the activated donut, and forms an anti-terminator hairpin (not shown). Thus, further transcription is aborted, thereby precluding protein translation that would up-regulate Trp biosynthesis. This simple feedback mechanism prevents excessive accumulation of free Trp. Images generated using Qutemol [9].

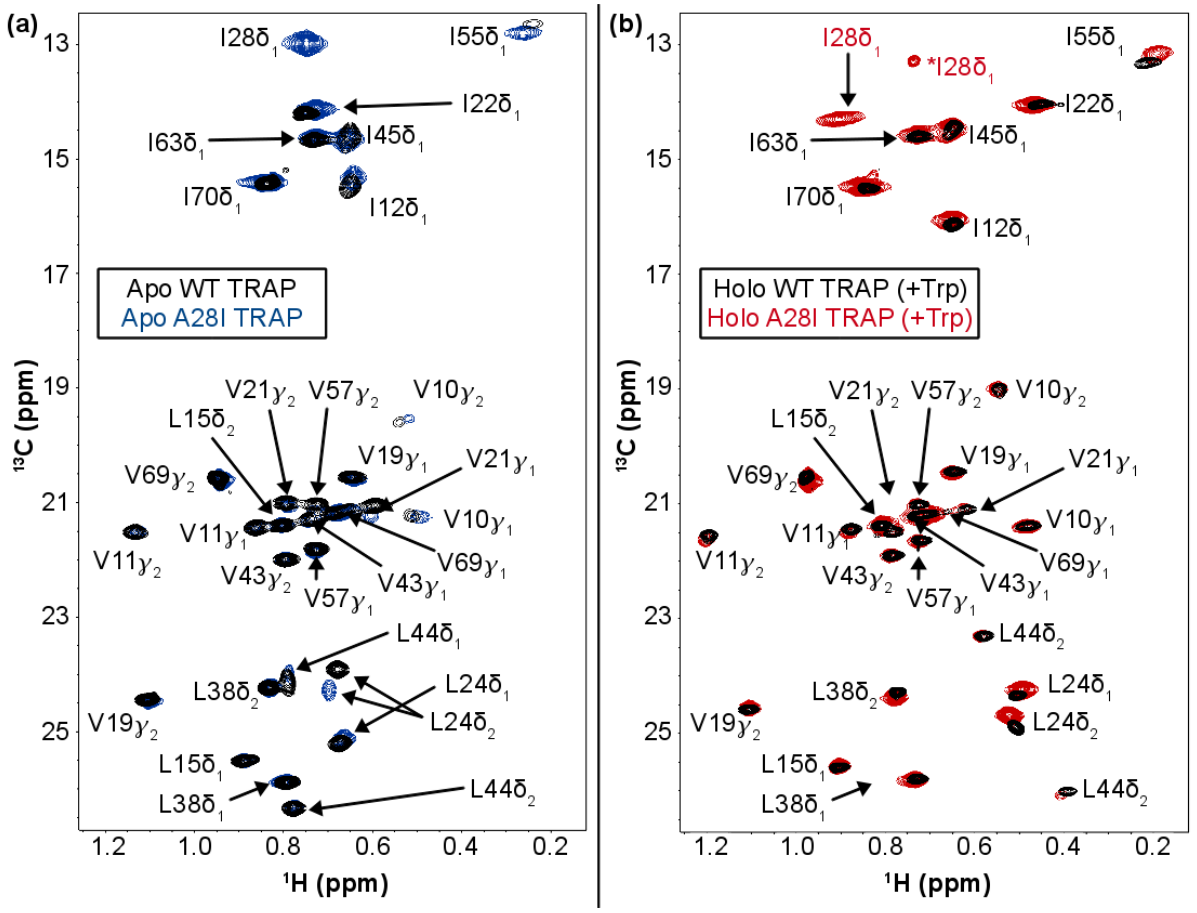

Fig. S2. The mutation Ala 28 to Ile, which introduces an additional methyl probe in the Trp-binding BC loop, does not significantly alter structure of apo nor holo TRAP. (a) Overlay of ^{1}H-^{13}C correlation spectra of apo TRAP at 25°C from WT (black) and A28I mutant (blue). The largest chemical shift perturbation upon mutation is at L24δ_2 near (δ_H, δ_C) = (0.7, 24) ppm. (b) The same overlay in the presence of Trp with WT (black) and A28I (red) also reveals no significant structural change upon mutation.

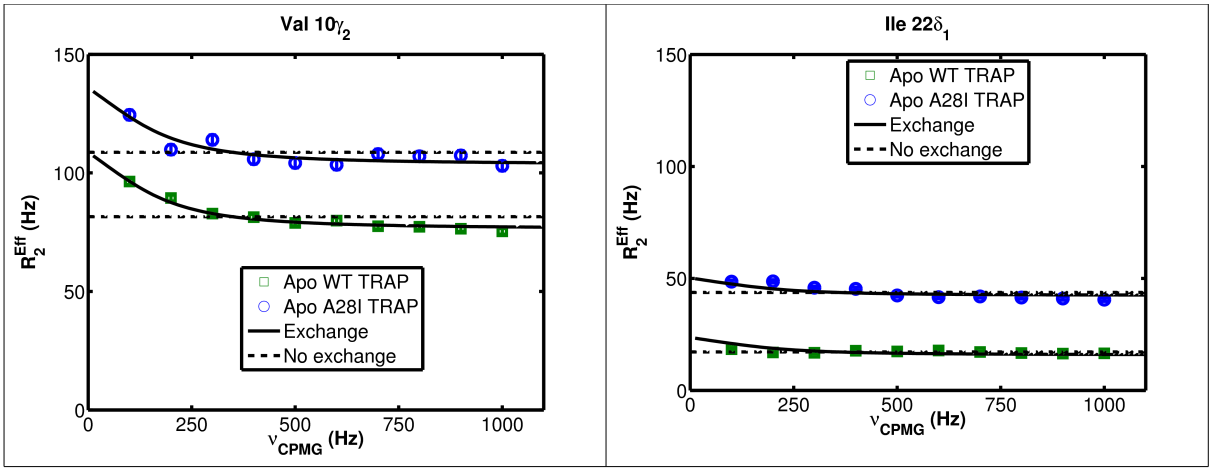

Fig. S3. Apo WT and A28I TRAP exhibit similar μs-ms dynamics based on $^{1}H,^{13}C$-MQ MRD experiments at 25°C at 600 MHz ^{1}H field. Results from two methyl groups are shown, which are representative of remaining results. Note that R_{ex} is the same in each, despite the difference in R_2^0 (i.e., $R_2^{Eff}(\nu_{CPMG}^{\infty})$).

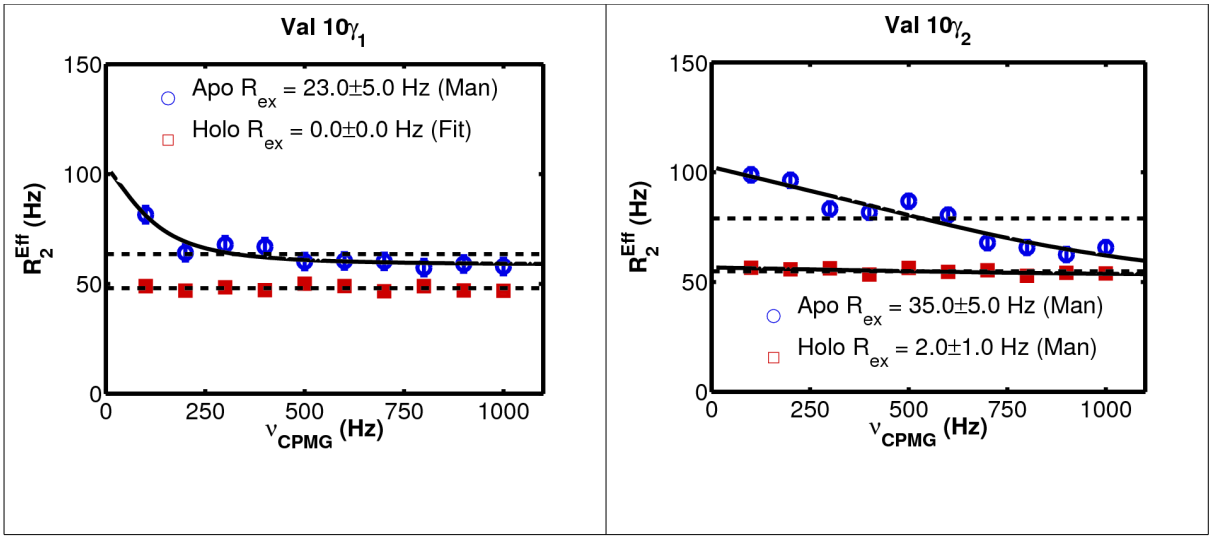

Fig. S4. MRD curves for each of 29 signals in apo and 30 signals in holo TRAP from ^{13}C-SQ MRD at 25°C. The exchange broadening is a simple metric to quantify µs-ms dynamics, and can be estimated from the fitted dispersion, $R_{ex} = R_2^{Eff}(\nu_{CPMG}^{0}) - R_2^{Eff}(\nu_{CPMG}^{\infty})$, designated in the legend by "(Fit)". However, some fits over-estimated R_{ex} (e.g., Val 21γ_2), and therefore were manually reduced based on the $R_{2,Eff}$ values observed at 100 Hz and 1000 Hz, designated in the legend by "(Man)". Since R_{ex} is reduced upon addition of Trp for nearly all methyl probes, the protein appears rigidified in the µs-ms time window. Note: $R_{ex}^{(holo)}$ is zero for all but 7 methyls, except Val 11γ_1, Ile 22δ_1, Val 43γ_1, Ile 45δ_1, and Val 69γ_1, with maximum value ~6 /sec for Ile 22δ_1 and Ile 45δ_1. Solid lines are fits to the site-specific two-state exchange model and dashed lines are fits to the no-exchange model. Note: due to signal overlap for two methyl pairs in the holo TRAP spectrum (Leu 15δ_2 with Val 21γ_2, and Val 43γ_1 with Val 69γ_1), the dispersion curve for each of the combined signal is presented. Because $R_2^{Eff}(\nu_{CPMG})$ does not decrease with ν_{CPMG} for SQ RD experiments, the combined signal yields an upper-limit estimate of

R_{ex} for the two overlapping signals (in these cases, R_{ex} is near zero).

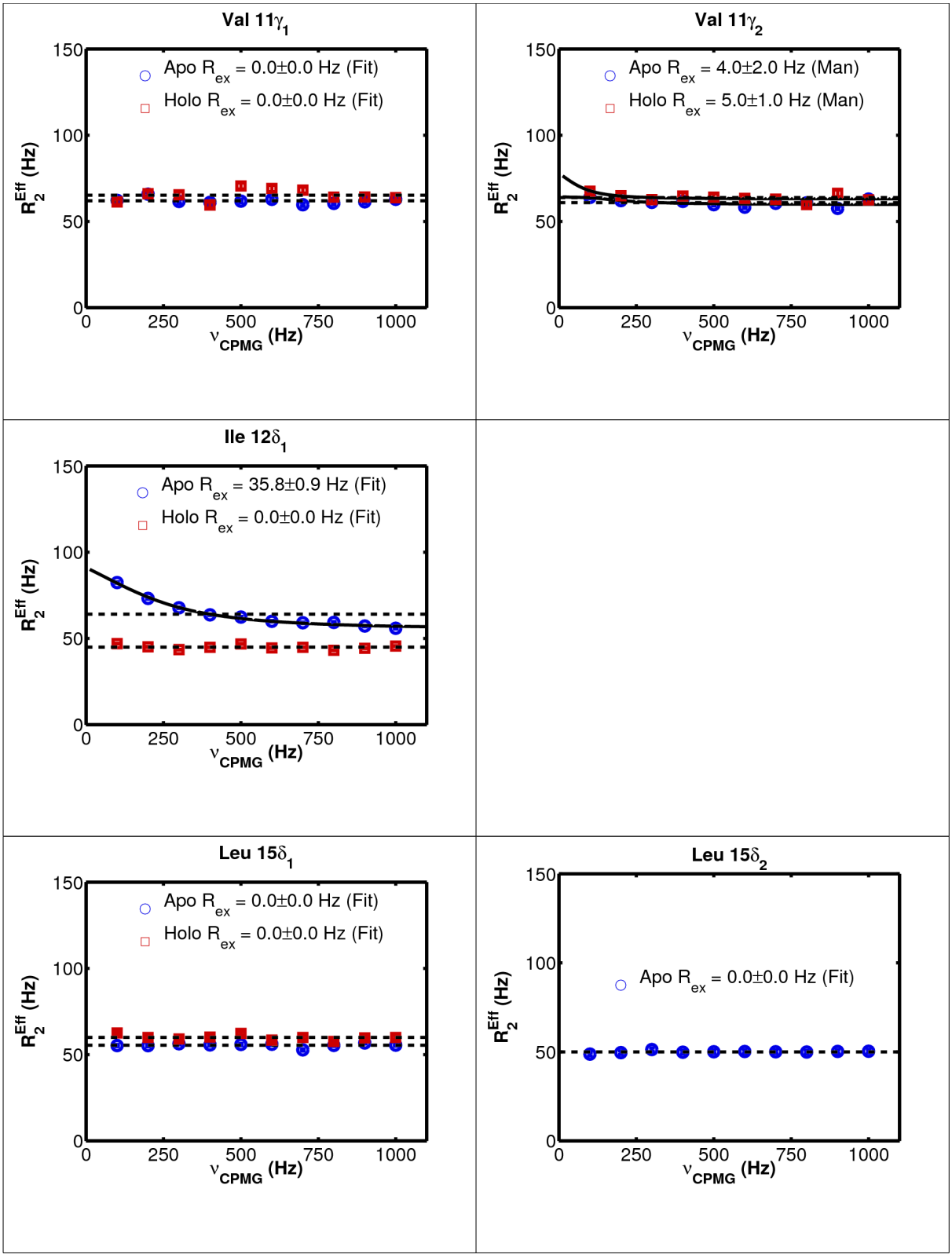
Val 11γ1
Apo Rex = 0.0±0.0 Hz (Fit)
Holo Rex = 0.0±0.0 Hz (Fit)
Val 11γ2
Apo Rex = 4.0±2.0 Hz (Man)
Holo Rex = 5.0±1.0 Hz (Man)
Ile 12δ1
Apo Rex = 35.8±0.9 Hz (Fit)
Holo Rex = 0.0±0.0 Hz (Fit)
Leu 15δ1
Apo Rex = 0.0±0.0 Hz (Fit)
Holo Rex = 0.0±0.0 Hz (Fit)
Leu 15δ2
Apo Rex = 0.0±0.0 Hz (Fit)
R2Eff (Hz)
νCPMG (Hz)
0
50
100
150
250
500
750
1000

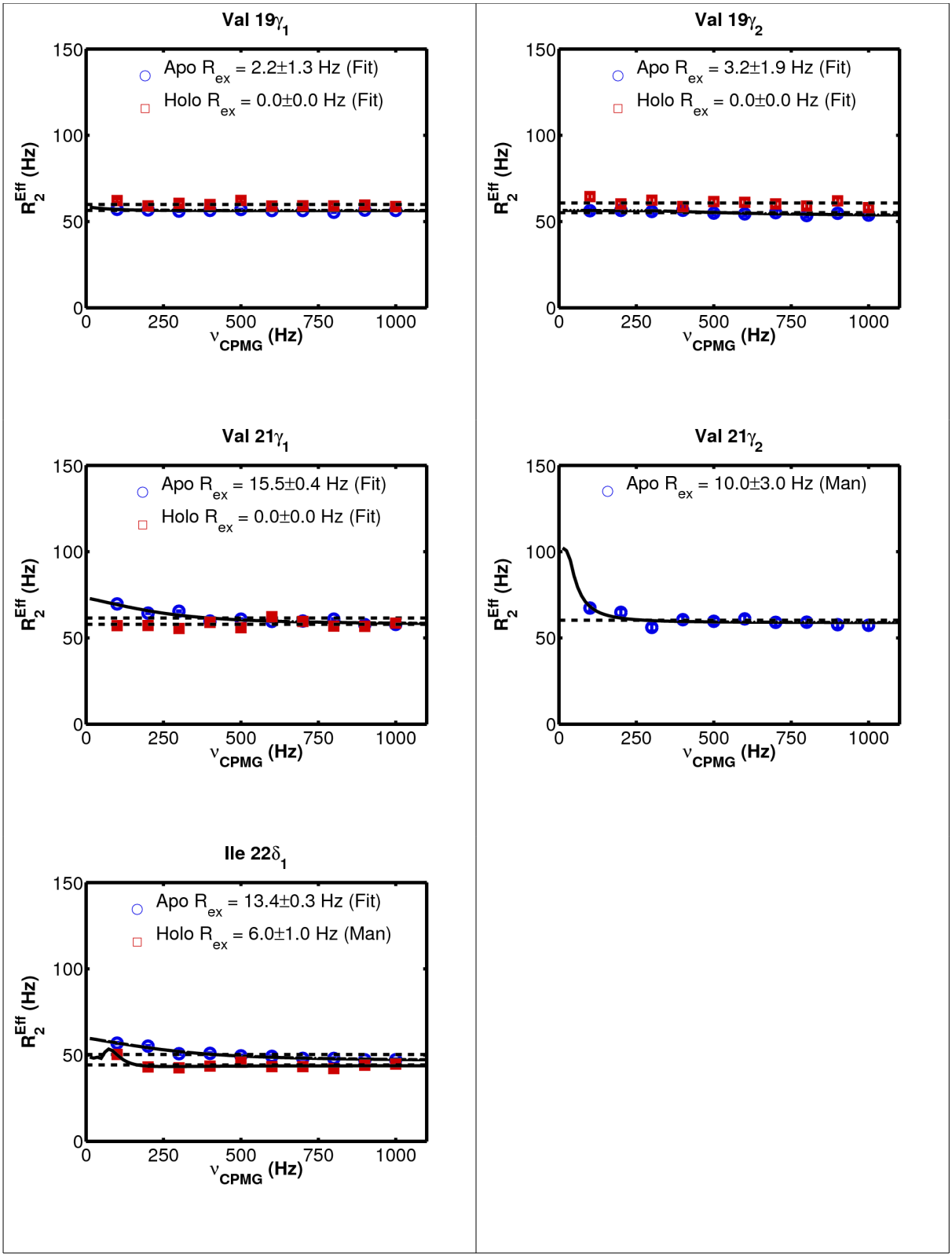
Val 19γ1
Apo Rex = 2.2±1.3 Hz (Fit)
Holo Rex = 0.0±0.0 Hz (Fit)
Val 19γ2
Apo Rex = 3.2±1.9 Hz (Fit)
Holo Rex = 0.0±0.0 Hz (Fit)
Val 21γ1
Apo Rex = 15.5±0.4 Hz (Fit)
Holo Rex = 0.0±0.0 Hz (Fit)
Val 21γ2
Apo Rex = 10.0±3.0 Hz (Man)
Ile 22δ1
Apo Rex = 13.4±0.3 Hz (Fit)
Holo Rex = 6.0±1.0 Hz (Man)
R2Eff (Hz)
νCPMG (Hz)
0
50
100
150
250
500
750
1000

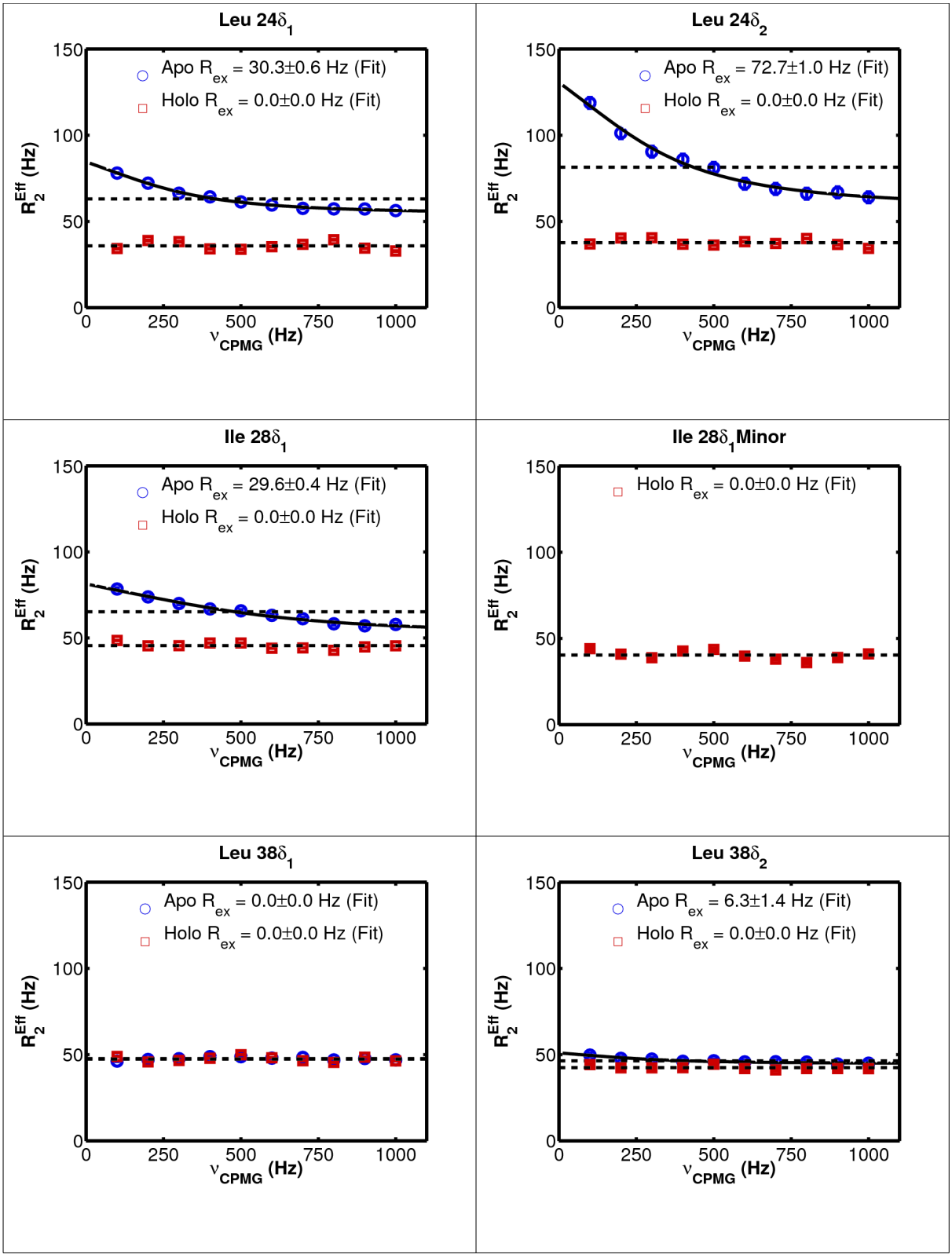
Leu 24δ1
Apo Rex = 30.3±0.6 Hz (Fit)
Holo Rex = 0.0±0.0 Hz (Fit)
Leu 24δ2
Apo Rex = 72.7±1.0 Hz (Fit)
Holo Rex = 0.0±0.0 Hz (Fit)
Ile 28δ1
Apo Rex = 29.6±0.4 Hz (Fit)
Holo Rex = 0.0±0.0 Hz (Fit)
Ile 28δ1Minor
Holo Rex = 0.0±0.0 Hz (Fit)
Leu 38δ1
Apo Rex = 0.0±0.0 Hz (Fit)
Holo Rex = 0.0±0.0 Hz (Fit)
Leu 38δ2
Apo Rex = 6.3±1.4 Hz (Fit)
Holo Rex = 0.0±0.0 Hz (Fit)
R2Eff (Hz)
νCPMG (Hz)
0
50
100
150
250
500
750
1000

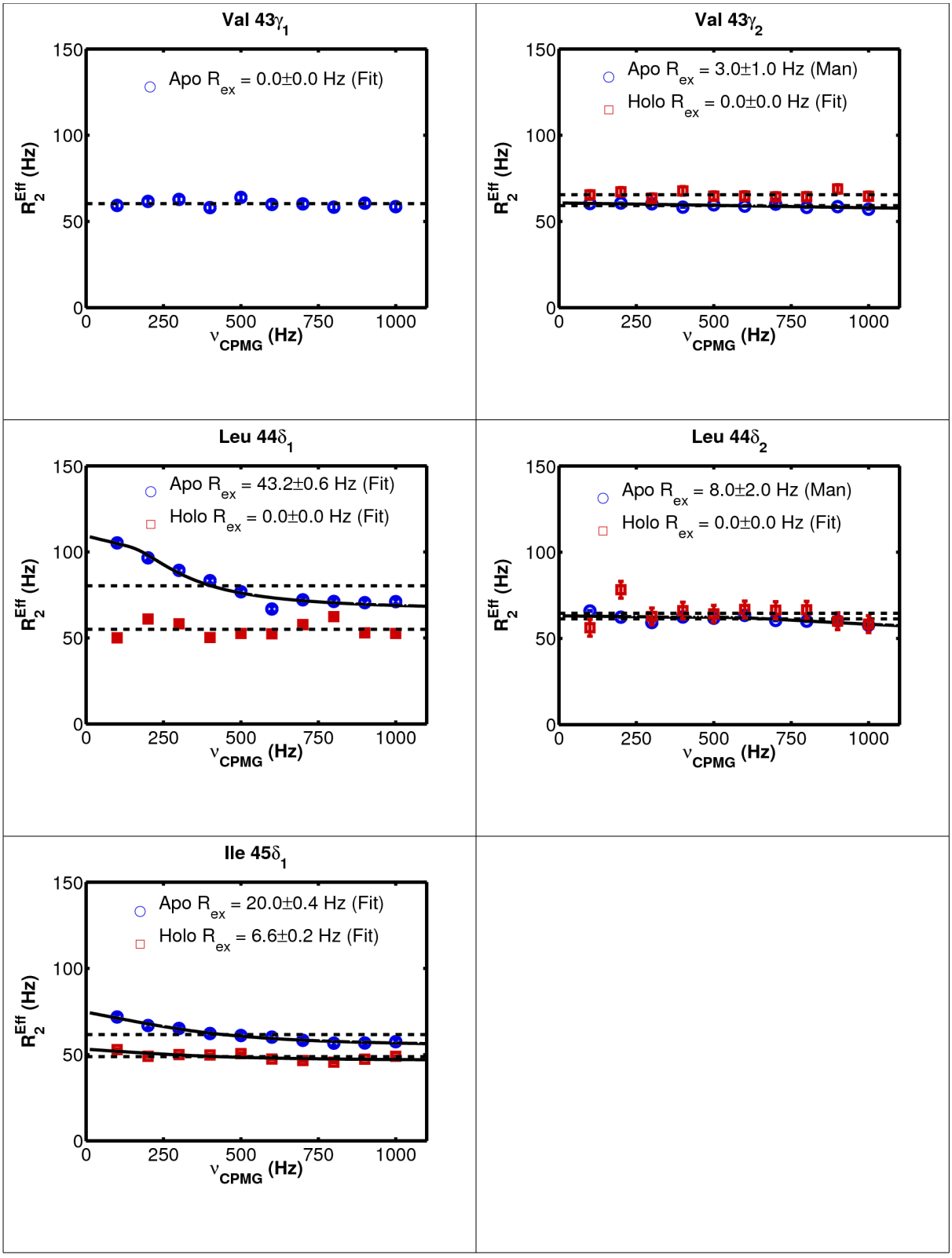
Val 43γ1
Apo Rex = 0.0±0.0 Hz (Fit)
Val 43γ2
Apo Rex = 3.0±1.0 Hz (Man)
Holo Rex = 0.0±0.0 Hz (Fit)
Leu 44δ1
Apo Rex = 43.2±0.6 Hz (Fit)
Holo Rex = 0.0±0.0 Hz (Fit)
Leu 44δ2
Apo Rex = 8.0±2.0 Hz (Man)
Holo Rex = 0.0±0.0 Hz (Fit)
Ile 45δ1
Apo Rex = 20.0±0.4 Hz (Fit)
Holo Rex = 6.6±0.2 Hz (Fit)
R2Eff (Hz)
νCPMG (Hz)
0
50
100
150
250
500
750
1000

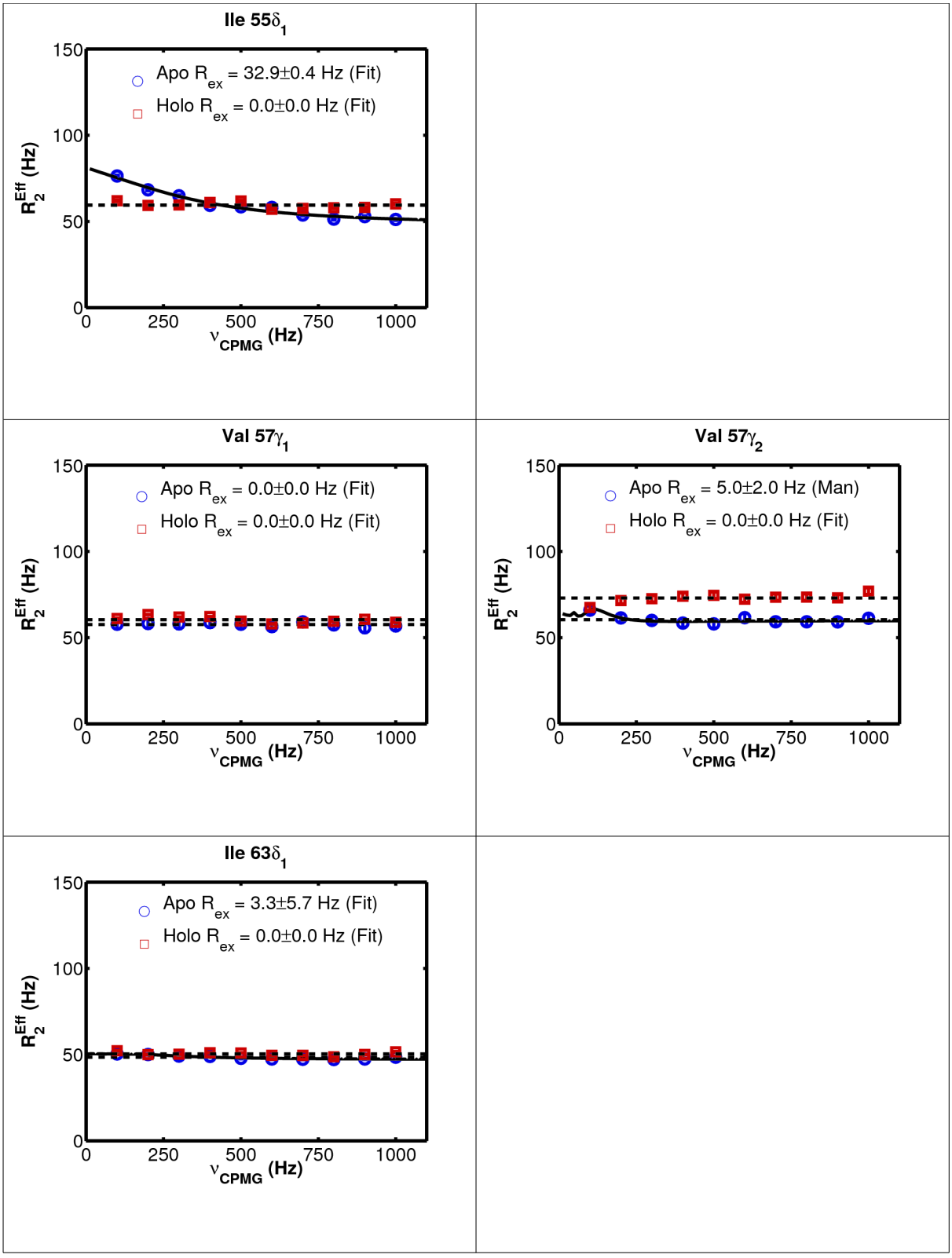
Ile 55δ1
Apo Rex = 32.9±0.4 Hz (Fit)
Holo Rex = 0.0±0.0 Hz (Fit)
Val 57γ1
Apo Rex = 0.0±0.0 Hz (Fit)
Holo Rex = 0.0±0.0 Hz (Fit)
Val 57γ2
Apo Rex = 5.0±2.0 Hz (Man)
Holo Rex = 0.0±0.0 Hz (Fit)
Ile 63δ1
Apo Rex = 3.3±5.7 Hz (Fit)
Holo Rex = 0.0±0.0 Hz (Fit)
R2Eff (Hz)
νCPMG (Hz)
0
50
100
150
250
500
750
1000

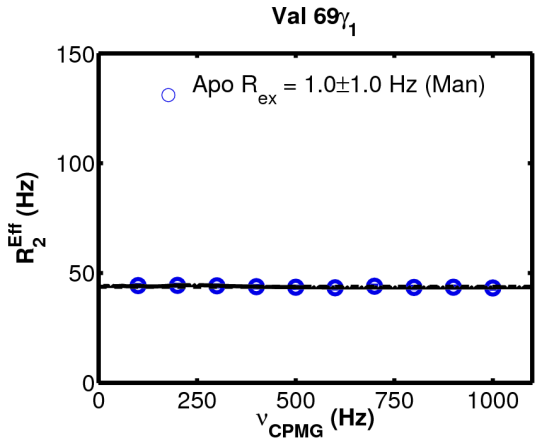
Val 69γ1
Apo Rex = 1.0±1.0 Hz (Man)
R2Eff (Hz)
νCPMG (Hz)
0
50
100
150
0
250
500
750
1000

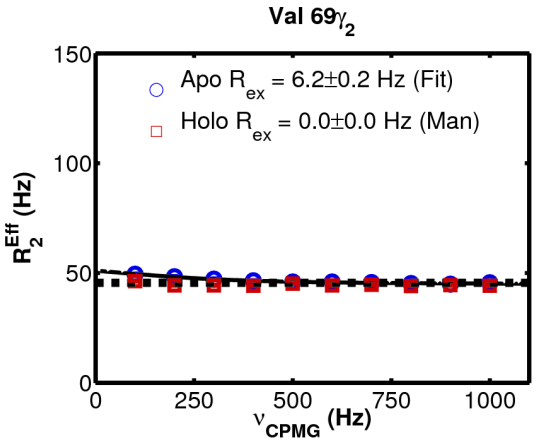
Val 69γ2
Apo Rex = 6.2±0.2 Hz (Fit)
Holo Rex = 0.0±0.0 Hz (Man)
R2Eff (Hz)
νCPMG (Hz)
0
50
100
150
0
250
500
750
1000

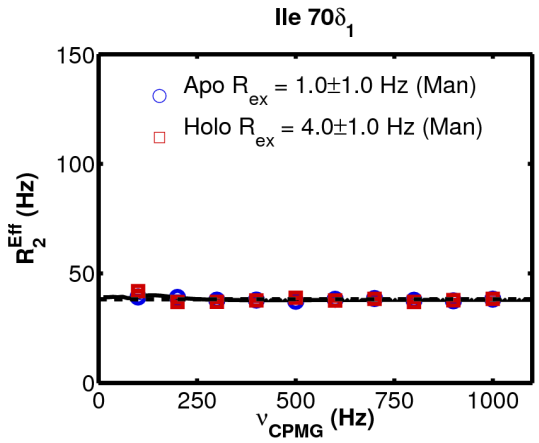
Ile 70δ1
Apo Rex = 1.0±1.0 Hz (Man)
Holo Rex = 4.0±1.0 Hz (Man)
R2Eff (Hz)
νCPMG (Hz)
0
50
100
150
0
250
500
750
1000

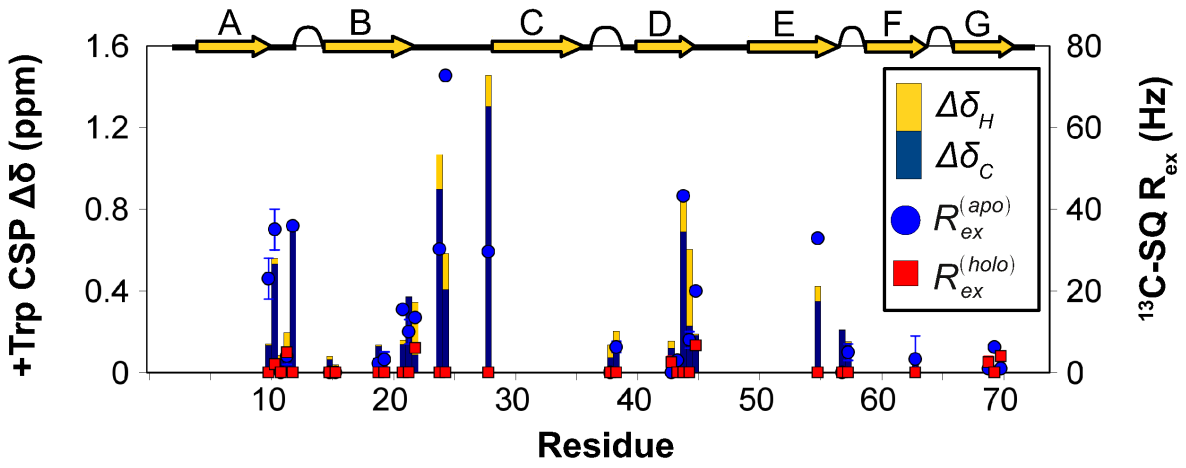

Fig. S5. Four site-specific NMR parameters are obtained for each of 29 methyl probes on the Ile, Leu, and Val side chains of TRAP. These probes provide reasonable coverage across the 74 residue sequence. (1, 2) ^{1}H and ^{13}C CSPs upon Trp-binding at 25°C, $\Delta\delta_H$ and $\Delta\delta_C$, reflect the magnitudes of site-specific structural differences between apo and holo TRAP. (3, 4) Exchange broadening from ^{13}C-SQ MRD at 25°C, $R_{ex}^{(apo)}$ and $R_{ex}^{(holo)}$, indicate significant mobility of apo TRAP and rigidity of holo TRAP in the μs-ms time window. Note that Trp-binding increases R_{ex} by a mere 2-3 /sec for three methyls (Ile 70δ_1, Val 43γ_2, and/or Val 69γ_2). Changes in structure and dynamics may be required to activate TRAP for RNA-binding. The secondary structure of holo TRAP is shown above the sequence, calculated using DSSP [22] with crystal structure PDB ID 1C9S [8].

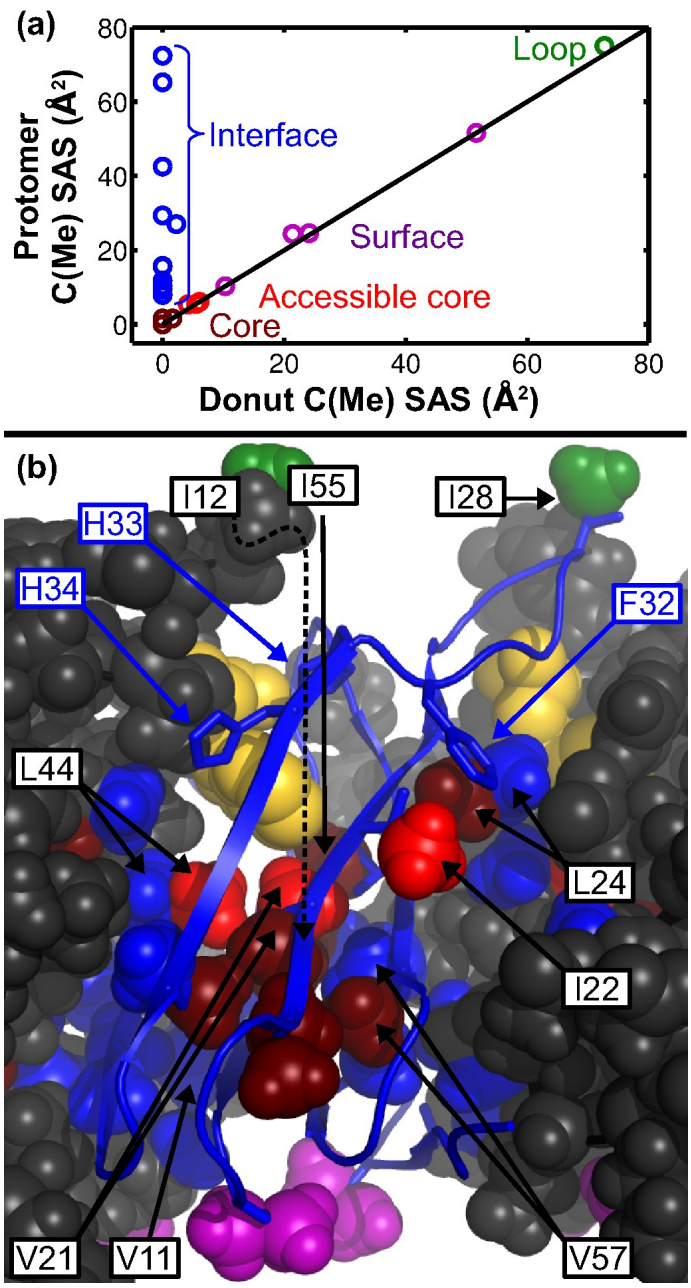

Fig. S6. Structural categorization methyls based on the surface accessibility of methyl carbons in the intact TRAP donut and in an isolated protomer, using GETAREA [10] and holo TRAP structure 1C9S [8] (n.b., similar groupings are obtained using apo TRAP crystal 3AQD [23]). The core exhibits nearly zero accessibility in both donut and protomer and contains 9 methyls: Val 10γ_2, Ile 12δ_1, Val 19γ_1, Val 19γ_2, Val 21γ_2, Leu 24δ_1, Leu 38δ_1, Ile 55δ_1, and Val 57γ_1. The accessible core exhibits small accessibility in both donut and protomer and contains 3 methyls: Val 21γ_1, Ile 22δ_1, and Leu 44δ_2. The interface exhibits nearly zero accessibility in the donut, but increased accessibility in the protomer (i.e., the neighboring protomer buries these methyls) and contains 12 methyls: Val 10γ_1, Val 11γ_1, Val 11γ_2, Leu 24δ_2, Leu 38δ_2, Val 43γ_1, Val 43γ_2, Leu 44δ_1, Ile 45δ_1, Val 57γ_2, Ile 63δ_1, and Ile 70δ_1. The surface exhibits nearly identical accessibility in the donut and the protomer, therefore following the black line of slope unity, and contains 4 methyls: Leu 15δ_1, Leu 15δ_2, Val 69γ_1, and

Val 69γ_2, with a special case at the Trp loop with 1 methyl: Ile 28δ_1.

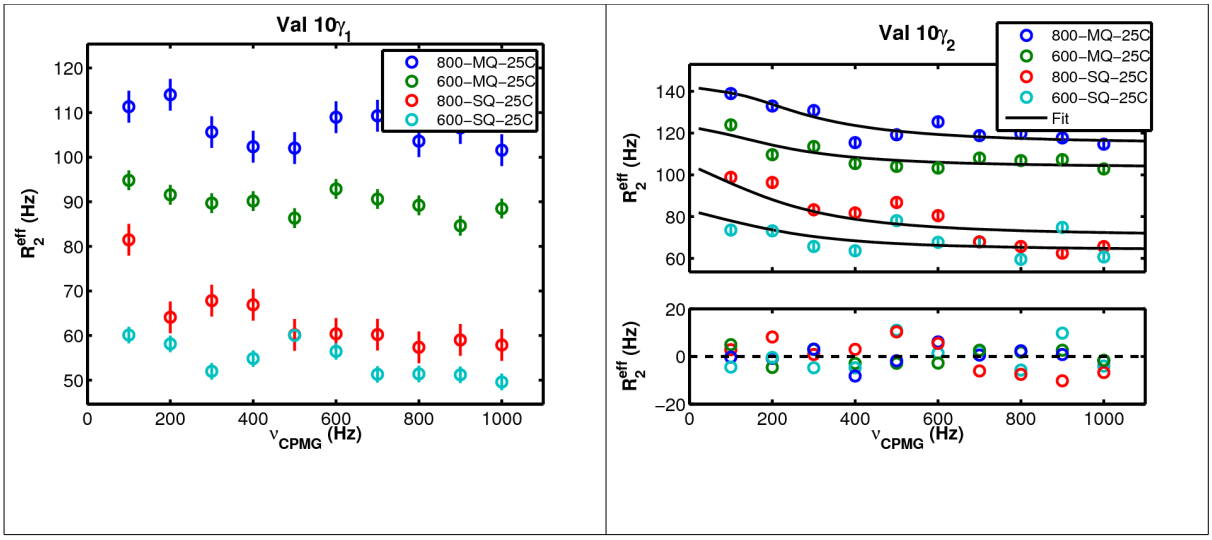

Figure S7. MRD data, and best fits to either the site-specific two-state exchange model or the model of no-exchange (horizontal lines) for each signal in apo TRAP. In this site-specific fit, each group of curves shares a common and optimized set of $|\Delta\omega_H|$, $|\Delta\omega_C|$, P_A, and k_{ex}, as well as one optimized R_2^0 unique for each curve. Residuals are shown in a subplot below each available fit, wherein a random distribution about zero indicates a reasonable fit to the data. Note: some groups exhibit exchange, but cannot be accurately fit due to poor signal to noise (e.g., Val 10γ_1).

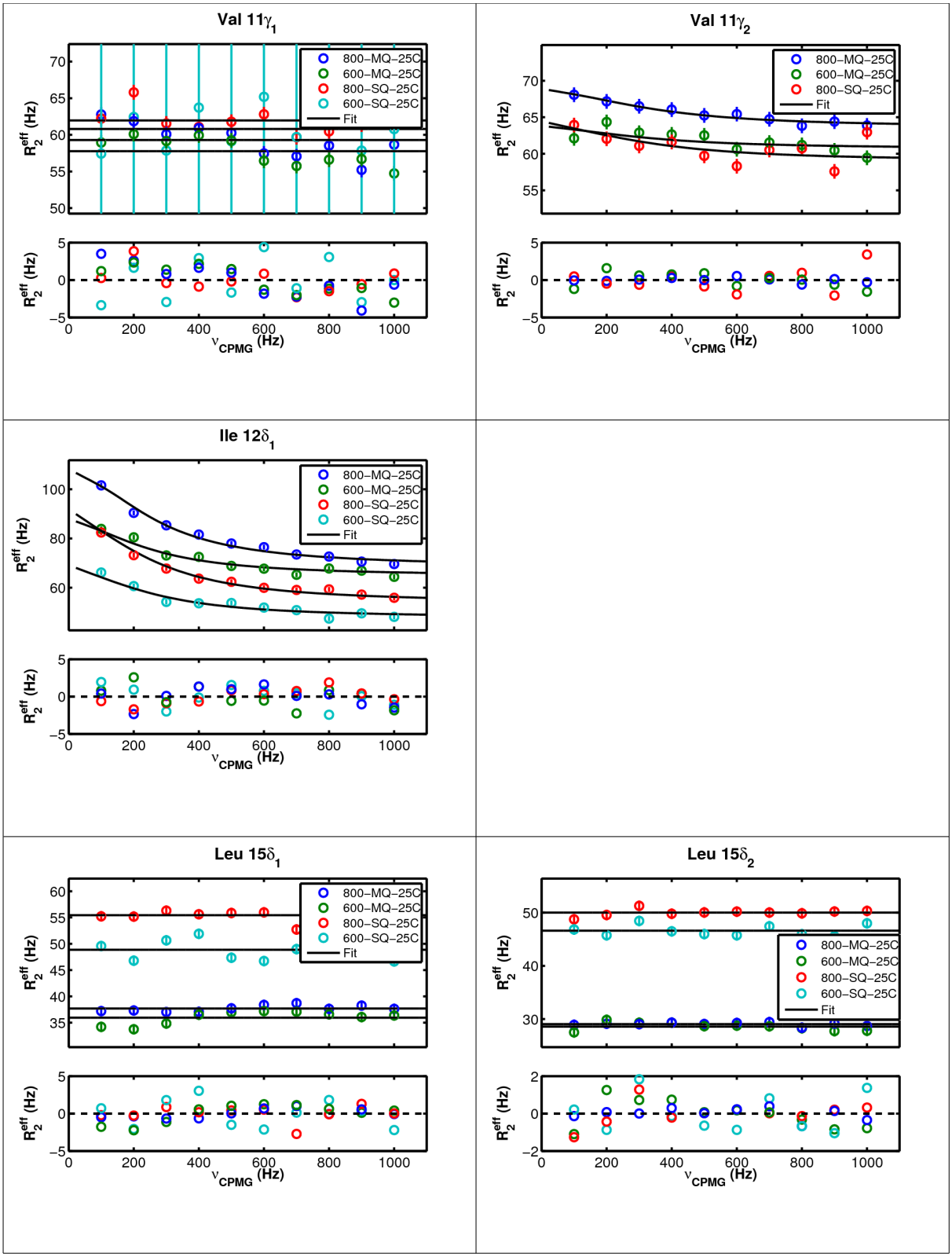
Val 11γ1
Val 11γ2
Ile 12δ1
Leu 15δ1
Leu 15δ2
800−MQ−25C
600−MQ−25C
800−SQ−25C
600−SQ−25C
Fit
R2eff (Hz)
νCPMG (Hz)

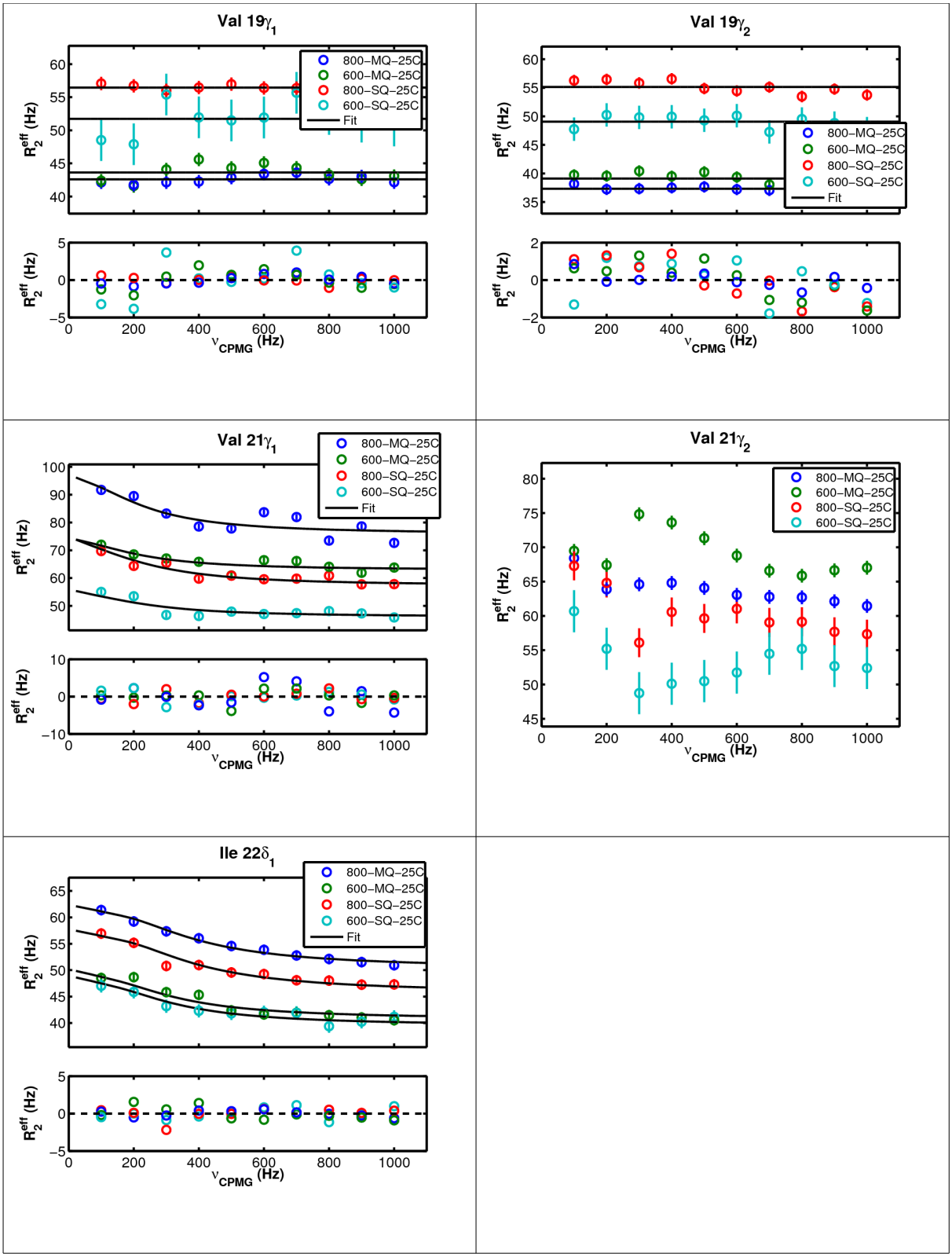
Val 19γ1
Val 19γ2
Val 21γ1
Val 21γ2
Ile 22δ1
800–MQ–25C
600–MQ–25C
800–SQ–25C
600–SQ–25C
Fit
R2eff (Hz)
νCPMG (Hz)

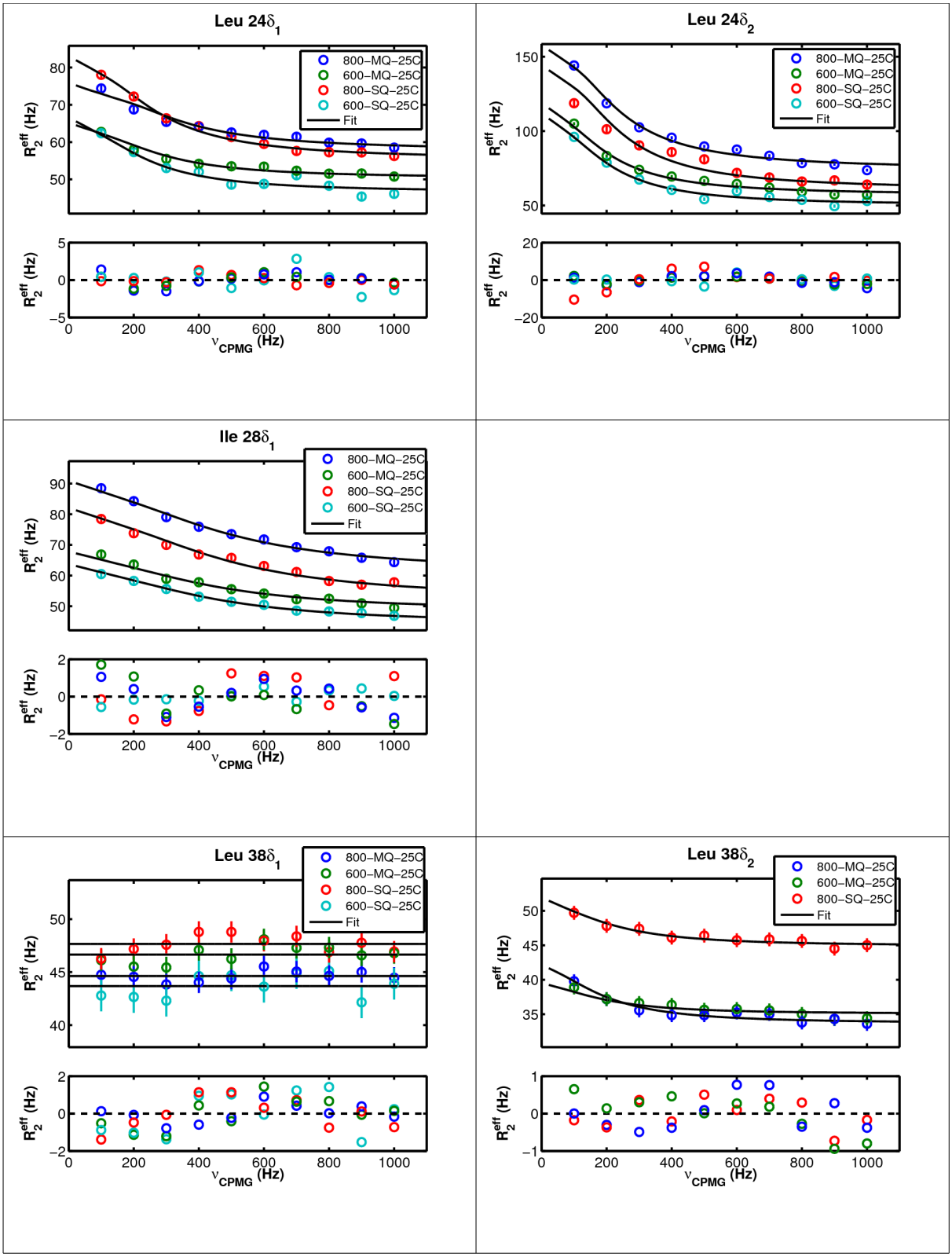
Leu 24δ1
Leu 24δ2
Ile 28δ1
Leu 38δ1
Leu 38δ2
800–MQ–25C
600–MQ–25C
800–SQ–25C
600–SQ–25C
Fit
R2eff (Hz)
νCPMG (Hz)

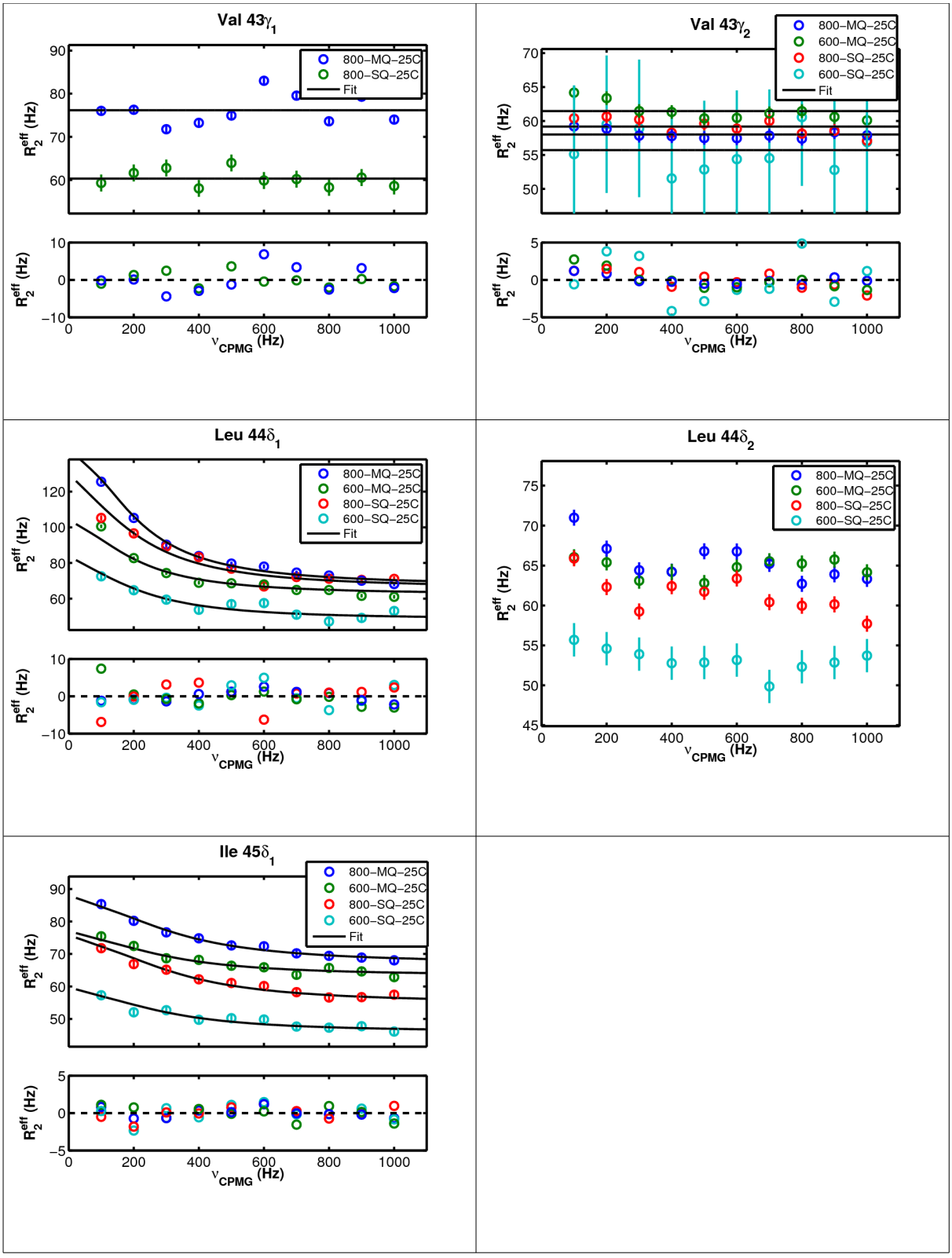
Val 43γ1
800–MQ–25C
800–SQ–25C
Fit
R2eff (Hz)
νCPMG (Hz)
Val 43γ2
800–MQ–25C
600–MQ–25C
800–SQ–25C
600–SQ–25C
Fit
R2eff (Hz)
νCPMG (Hz)
Leu 44δ1
800–MQ–25C
600–MQ–25C
800–SQ–25C
600–SQ–25C
Fit
R2eff (Hz)
νCPMG (Hz)
Leu 44δ2
800–MQ–25C
600–MQ–25C
800–SQ–25C
600–SQ–25C
R2eff (Hz)
νCPMG (Hz)
Ile 45δ1
800–MQ–25C
600–MQ–25C
800–SQ–25C
600–SQ–25C
Fit
R2eff (Hz)
νCPMG (Hz)

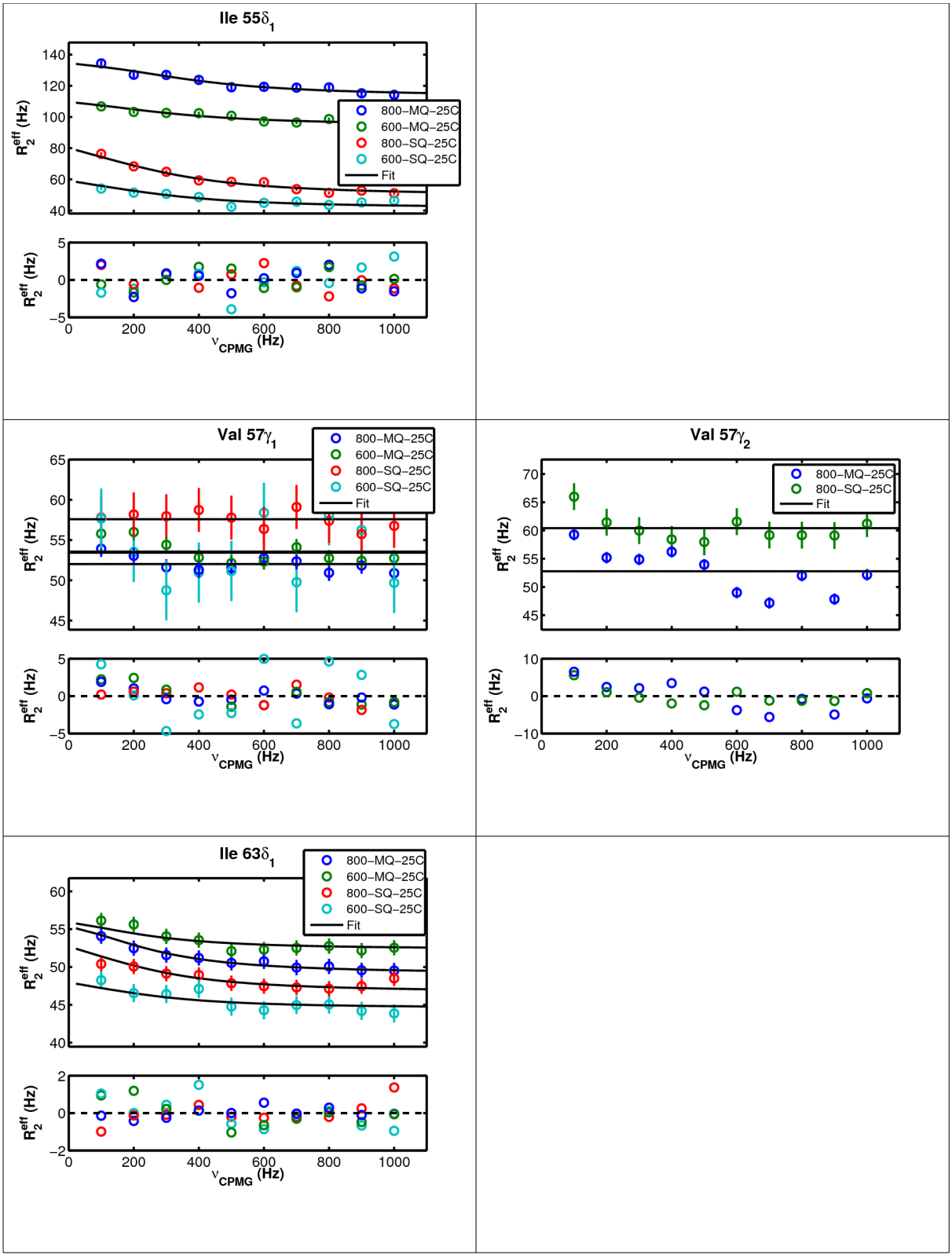
Ile 55δ1
800–MQ–25C
600–MQ–25C
800–SQ–25C
600–SQ–25C
Fit
R2eff (Hz)
νCPMG (Hz)
Val 57γ1
Val 57γ2
Ile 63δ1

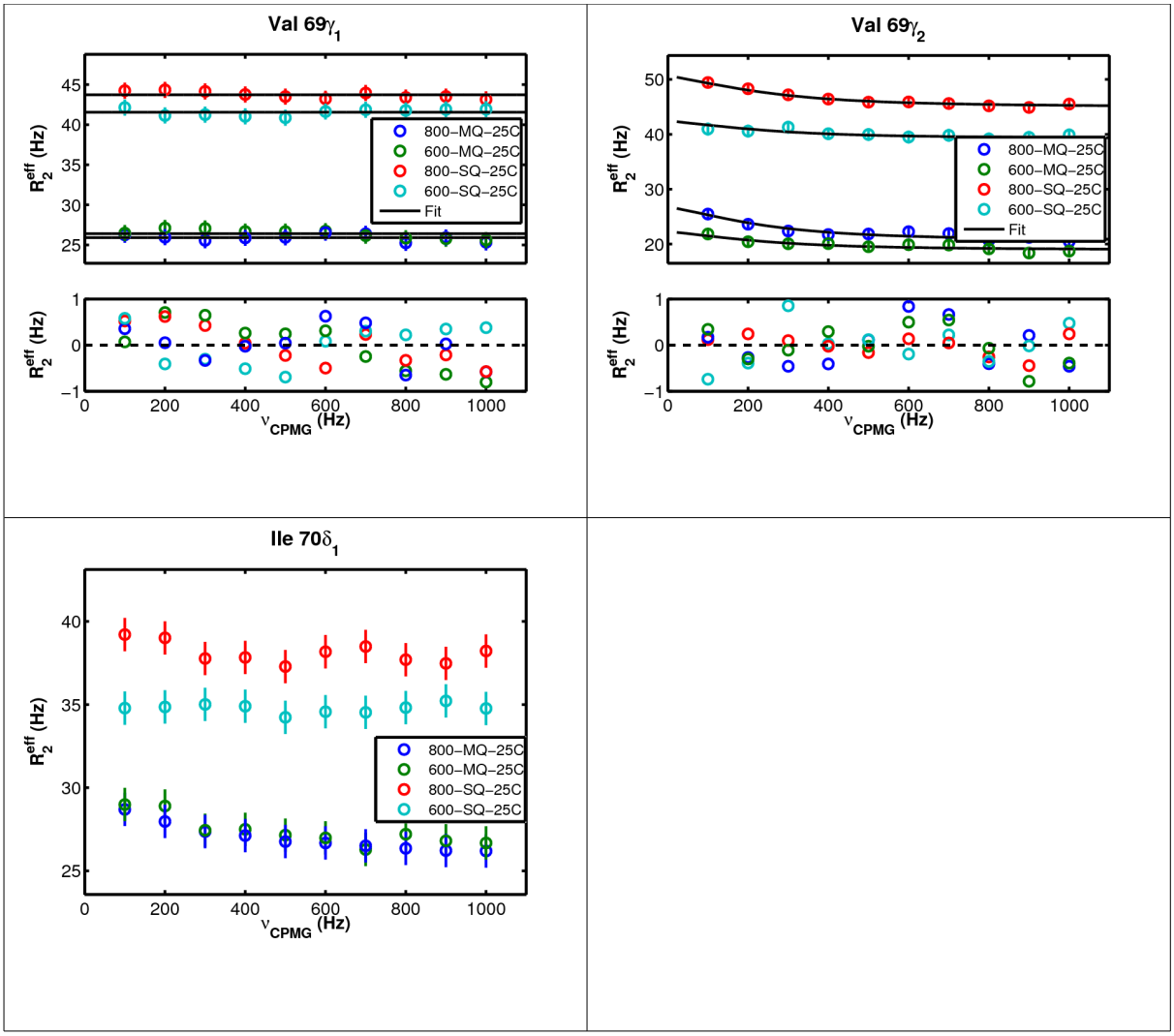
Val 69γ1
Val 69γ2
Ile 70δ1
800−MQ−25C
600−MQ−25C
800−SQ−25C
600−SQ−25C
Fit
R2eff (Hz)
νCPMG (Hz)

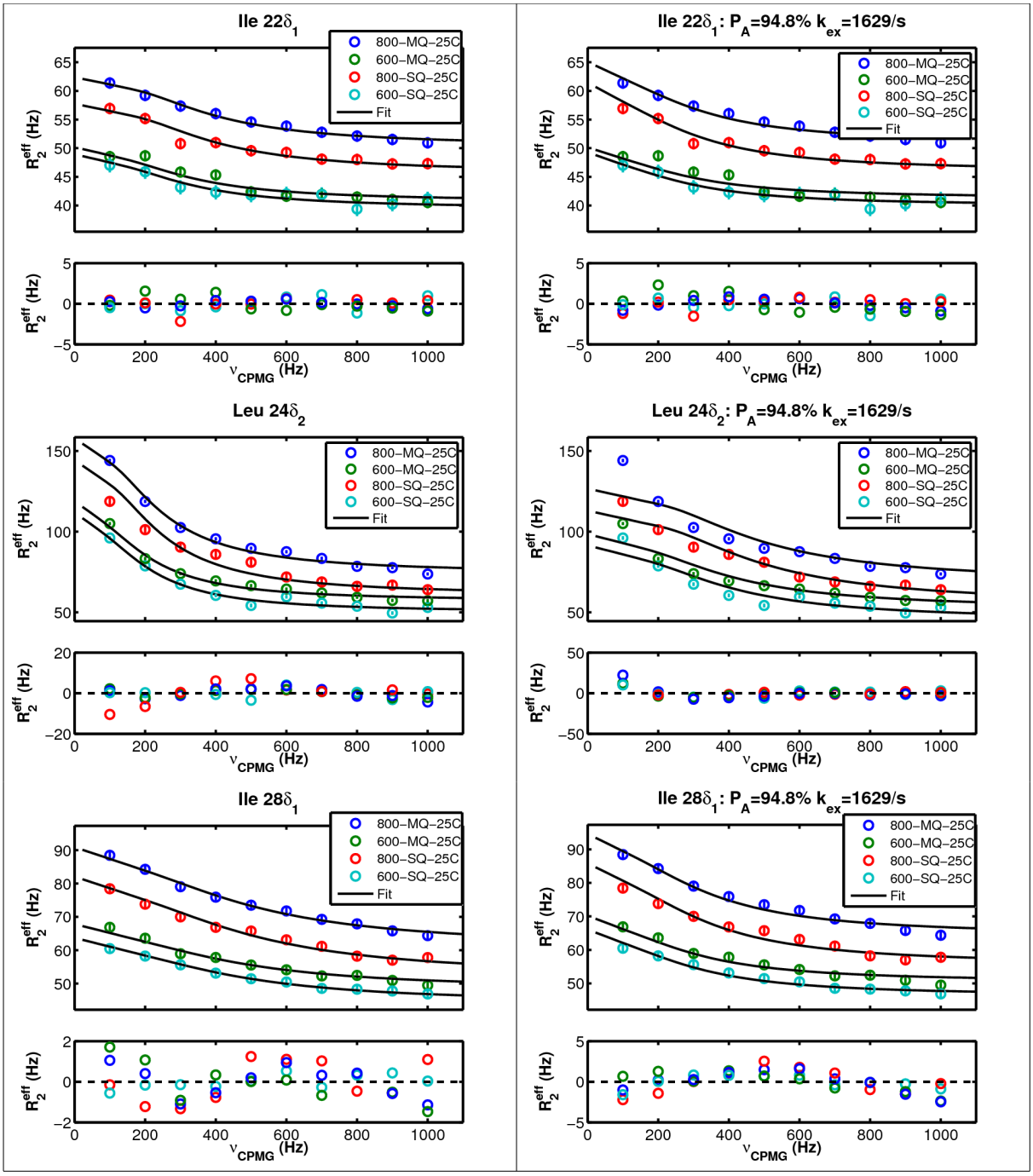

Fig. S8. A global fit which fixes k_{ex} and P_A to their average values, while optimizing site-specific $|\Delta\omega_H|$, $|\Delta\omega_C|$, and R_2^0 , yields inaccurate fits for probes far from this average, as evidenced by larger and systematic residuals. For each of Ile 22δ_1, Leu 24δ_2, and Ile 28δ_1, the optimized fits and residuals are shown when k_{ex} and P_A are

site-specific parameters (left) and when they are fixed to the global average (right).

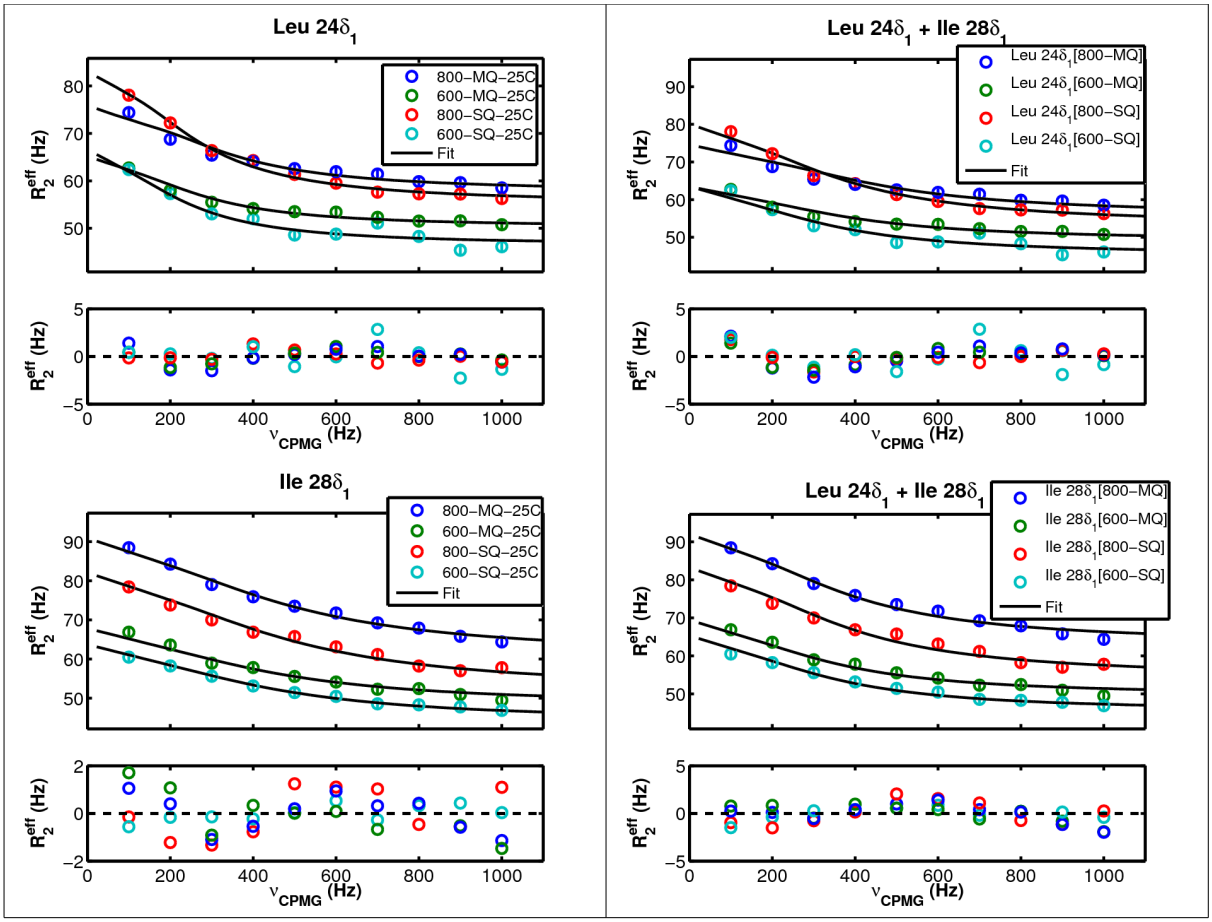

Fig. S9. The fastest exchanging probe in apo TRAP, Ile 28δ_1, and either of the two slowest-exchanging probes, Leu 24δ_1 (four figures above) or Leu 24δ_2 (four figures below), are not well-described by a global dynamic process because they exhibit different values for each of k_{ex} and P_A. (Left) The isolated fits of each probe yield randomly distributed residuals, which are consistent with a reliable fit. (Right) The global fit of the two probes to a shared and optimized k_{ex} and P_A pair yield systematic residuals, especially for Ile 28δ_1, which indicate a poor fit.

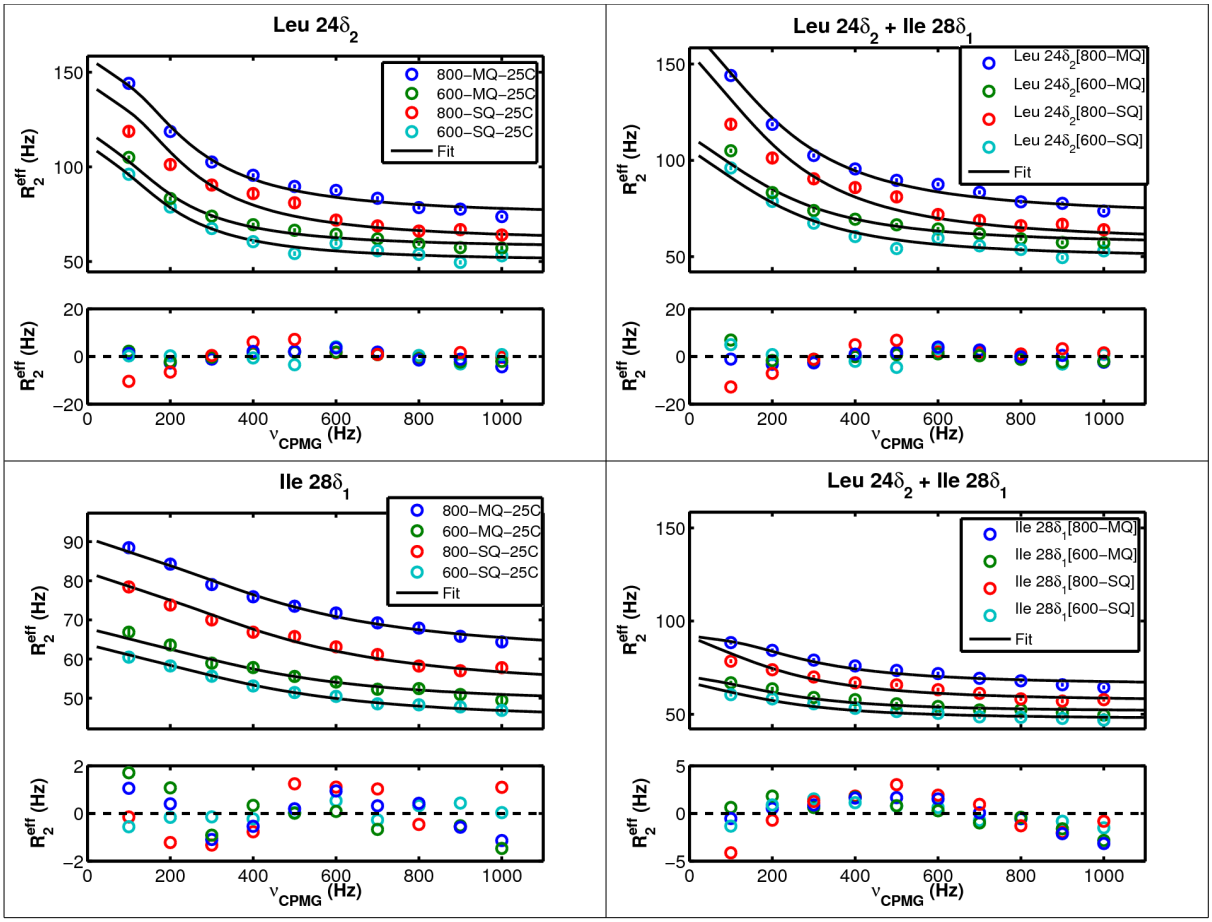
Leu 24δ2
800–MQ–25C
600–MQ–25C
800–SQ–25C
600–SQ–25C
Fit
Leu 24δ2 + Ile 28δ1
Leu 24δ2[800–MQ]
Leu 24δ2[600–MQ]
Leu 24δ2[800–SQ]
Leu 24δ2[600–SQ]
Fit
Ile 28δ1
800–MQ–25C
600–MQ–25C
800–SQ–25C
600–SQ–25C
Fit
Leu 24δ2 + Ile 28δ1
Ile 28δ1[800–MQ]
Ile 28δ1[600–MQ]
Ile 28δ1[800–SQ]
Ile 28δ1[600–SQ]
Fit
R2eff (Hz)
νCPMG (Hz)

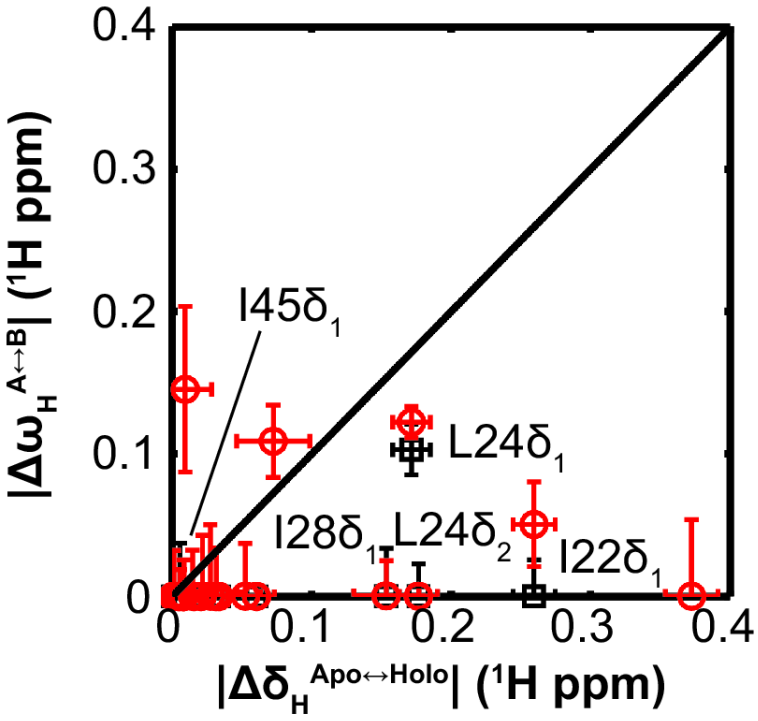

Fig. S10. ^{1}H chemical shift differences from apo TRAP MRD, $\Delta\omega_H$, are compared to ^{1}H CSPs upon Trp-binding, $\Delta\delta_H$ (note: this is the ^{1}H counterpart to the $\Delta\omega_C$ figure 4b in the main text). The site-specific fits to MRD data yield 5 reliable values for $|\Delta\omega_H|$ (black squares), whereas assuming "global" concerted motion yields 18 values (red circles; see main text for discussion). Since ^{1}H shifts are strongly dependent on through-space shielding effects [24], the Trp-induced CSPs, $\Delta\delta_H$, can be strongly affected by the ring current shift from the Trp ligand (e.g., L44δ_2 near bound Trp exhibits $\Delta\delta_H$ = 0.37 ppm). However, since apo TRAP contains no Trp, non-zero $\Delta\omega_H$ results from μs-ms methyl reorientation relative to other electron-rich functional groups, which may alter δ_H. As mentioned in the text, the chemical shifts and relaxation behavior of the methyl groups on Leu24, L24δ_1 and L24δ_2, probe different parts of the apo TRAP structure. Specifically, Leu 24δ_1 is pointed toward the protomer core in holo TRAP, and reports a large $|\Delta\omega_H|$ of 0.1±0.02 ppm in apo TRAP, which likely results from the aromatic sidechain of Phe 32. In contrast, Leu 24δ_2 is

pointed toward the inter-protomer interface in holo TRAP, and reports a near-zero |$\Delta\omega_H$| of 0±0.02 ppm.

References

[1] McElroy, C., Manfredo, A., Wendt, A., Gollnick, P. & Foster,M. (2002). Trosy-nmr studies of the 91kda trap protein reveal allosteric control of a gene regulatory protein by ligand-altered flexibility. *J. Mol. Biol.* **323**, pp. 463-473.

[2] Wilkins, M.R., Gasteiger, E., Bairoch, A., Sanchez, J.C., Williams, K.L., Appel, R.D. & Hochstrasser,D.F. (1999). Protein identification and analysis tools in the expasy server. *Methods Mol. Biol.* **112**, pp. 531-552.

[3] Fasman, G. (1976). Handbook of biochemistry and molecular biology, proteins, i. (), pp. 183-203, CRC Press, 3 ed., .

[4] Tugarinov, V. & Kay,L.E. (2003). Ile, leu, and val methyl assignments of the 723-residue malate synthase g using a new labeling strategy and novel nmr methods. *J. Am. Chem. Soc.* **125**, pp. 13868-13878.

[5] Senn, H., Werner, B., Messerele, B.A., Weber, C., Traber, R. & Wuthrich,K. (1989). Stereospecific assignment of the methyl h-1-nmr lines of valine and leucine in polypeptides by nonrandom c-13 labeling. *FEBS Lett.* **249**, pp. 113-118.

[6] Goto, N.K., Gardner, K.H., Mueller, G.A., Willis, R.C. & Kay,L.E. (1999). A robust and cost-effective method for the production of val, leu, ile (delta 1) methyl-protonated 15n-, 13c-, 2h-labeled proteins. *J. Biomol. NMR* **13**, pp. 369-374.

[7] McElroy, C.A., Manfredo, A., Gollnick, P. & Foster,M.P. (2006). Thermodynamics of tryptophan-mediated activation of the trp rna-binding attenuation protein. *Biochemistry* **45**, pp. 7844-7853.

[8] Antson, A.A., Dodson, E.J., Dodson, G., Greaves, R.B., Chen, X. & Gollnick,P. (1999). Structure of the trp rna-binding attenuation protein, trap, bound to rna.

Nature **401**, pp. 235-242.

[9] Tarini, M., Cignoni, P. & Montani,C. (2006). Ambient occlusion and edge cueing to enhance real time molecular visualization. *Ieee Trans Visual Comput Gr* **12**, p. IEEE-1244.

[10] Fraczkiewicz, R. & Braun,W. (1998). Exact and efficient analytical calculation of the accessible surface areas and their gradients for macromolecules. *J Comput Chem* **19**, pp. 319-333.

[11] Korzhnev, D.M., Kloiber, K., Kanelis, V., Tugarinov, V. & Kay,L.E. (2004). Probing slow dynamics in high molecular weight proteins by methyl-trosy nmr spectroscopy: application to a 723-residue enzyme. *J. Am. Chem. Soc.* **126**, pp. 3964-3973.

[12] Lundström, P., Vallurupalli, P., Religa, T.L., Dahlquist, F.W. & Kay,L.E. (2007). A single-quantum methyl 13c-relaxation dispersion experiment with improved sensitivity. *J. Biomol. NMR* **38**, pp. 79-88.

[13] Delaglio, F., Grzesiek, S., Vuister, G.W., Zhu, G., Pfeifer, J. & Bax,A. (1995). Nmrpipe: a multidimensional spectral processing system based on unix pipes. *J. Biomol. NMR* **6**, pp. 277-293.

[14] Johnson, B.A. & Blevins,R.A. (1994). Nmr view - a computer-program for the visualization and analysis of nmr data. *J. Biomol. NMR* **4**, pp. 603-614.

[15] Korzhnev, D.M., Kloiber, K. & Kay,L.E. (2004). Multiple-quantum relaxation dispersion nmr spectroscopy probing millisecond time-scale dynamics in proteins: theory and application. *J. Am. Chem. Soc.* **126**, pp. 7320-7329.

[16] Ishima, R. & Torchia,D.A. (2006). Accuracy of optimized chemical-exchange parameters derived by fitting cpmg r2 dispersion profiles when r2(0a) not = r2(0b). *J.*

Biomol. NMR **34**, pp. 209-219.

[17] Kovrigin, E.L., Kempf, J.G., Grey, M.J. & Loria,J.P. (2006). Faithful estimation of dynamics parameters from cpmg relaxation dispersion measurements. *J. Magn. Reson.* **180**, pp. 93-104.

[18] Ishima, R. & Torchia,D.A. (2005). Error estimation and global fitting in transverse-relaxation dispersion experiments to determine chemical-exchange parameters. *J. Biomol. NMR* **32**, pp. 41-54.

[19] Millet, O., Loria, J.P., Kroenke, C.D., Pons, M. & Palmer,A.G. (2000). The static magnetic field dependence of chemical exchange linebroadening defines the nmr chemical shift time scale. *J. Am. Chem. Soc.* **122**, pp. 2867-2877.

[20] Motulsky, H. & Christopoulos,A. (2003). Fitting models to biological data using linear and nonlinear regression. a practical guide to curve fitting.. (Graphpad Software Inc. (Ed.)), p. 104, Graphpad Software Inc., San Diego, CA.

[21] Schrodinger, L.. The pymol molecular graphics system, version~1.2r1.

[22] Kabsch, W. & Sander,C. (1983). Dictionary of protein secondary structure: pattern recognition of hydrogen-bonded and geometrical features. *Biopolymers* **22**, pp. 2577-2637.

[23] Malay, A.D., Watanabe, M., Heddle, J.G. & Tame,J.R.H. (2011). Crystal structure of unliganded trap: implications for dynamic allostery. *Biochem. J.* **434**, pp. 427-434.

[24] Wishart, D.S. & Case,D.A. (2001). Use of chemical shifts in macromolecular structure determination. *Meth. Enzymol.* **338**, pp. 3-34.